ISSN 1949-8470 (online)

World Journal of *Radiology*

World J Radiol 2019 March 28; 11(3): 27-54

Published by Baishideng Publishing Group Inc

WJR World Journal of Radiology

Contents

Monthly Volume 11 Number 3 March 28, 2019

MINIREVIEWS

Contents

World Journal of Radiology

Volume 11 Number 3 March 28, 2019

ABOUT COVER

Editorial Board Member of *World Journal of Radiology*, SeyedReza Najafizadeh, MD, Associate Professor, Department of Rheumatology, Imam Khomeini Hospital, Tehran University of Medical Sciences, Tehran 1586814116, Iran

AIMS AND SCOPE

World Journal of Radiology (*World J Radiol*, *WJR*, online ISSN 1949-8470, DOI: 10.4329) is a peer-reviewed open access academic journal that aims to guide clinical practice and improve diagnostic and therapeutic skills of clinicians.

The *WJR* covers topics concerning diagnostic radiology, radiation oncology, radiologic physics, neuroradiology, nuclear radiology, pediatric radiology, vascular/interventional radiology, medical imaging achieved by various modalities and related methods analysis. The current columns of *WJR* include editorial, frontier, mini-reviews, review, medical ethics, original articles, case report, *etc*.

We encourage authors to submit their manuscripts to *WJR*. We will give priority to manuscripts that are supported by major national and international foundations and those that are of great basic and clinical significance.

INDEXING/ABSTRACTING

The *WJR* is now abstracted and indexed in Emerging Sources Citation Index (Web of Science), PubMed, PubMed Central, China National Knowledge Infrastructure (CNKI), China Science and Technology Journal Database (CSTJ), and Superstar Journals Database.

RESPONSIBLE EDITORS FOR THIS ISSUE

Responsible Electronic Editor: *Yun-Xiaojian Wu* **Proofing Editorial Office Director:** *Jin-Lei Wang*

NAME OF JOURNAL
World Journal of Radiology

ISSN
ISSN 1949-8470 (online)

LAUNCH DATE
January 31, 2009

FREQUENCY
Monthly

EDITORS-IN-CHIEF
Venkatesh Mani

EDITORIAL BOARD MEMBERS
https://www.wjgnet.com/1949-8470/editorialboard.htm

EDITORIAL OFFICE
Jin-Lei Wang, Director

PUBLICATION DATE
March 28, 2019

INSTRUCTIONS TO AUTHORS
https://www.wjgnet.com/bpg/gerinfo/204

GUIDELINES FOR ETHICS DOCUMENTS
https://www.wjgnet.com/bpg/GerInfo/287

GUIDELINES FOR NON-NATIVE SPEAKERS OF ENGLISH
https://www.wjgnet.com/bpg/gerinfo/240

PUBLICATION MISCONDUCT
https://www.wjgnet.com/bpg/gerinfo/208

ARTICLE PROCESSING CHARGE
https://www.wjgnet.com/bpg/gerinfo/242

STEPS FOR SUBMITTING MANUSCRIPTS
https://www.wjgnet.com/bpg/GerInfo/239

ONLINE SUBMISSION
https://www.f6publishing.com

World Journal of Radiology

Submit a Manuscript: https://www.f6publishing.com

World J Radiol 2019 March 28; 11(3): 27-45

DOI: 10.4329/wjr.v11.i3.27

ISSN 1949-8470 (online)

MINIREVIEWS

Role of advanced magnetic resonance imaging in the assessment of malignancies of the mediastinum

Jordi Broncano, Ana María Alvarado-Benavides, Sanjeev Bhalla, Antonio Álvarez-Kindelan, Constantine A Raptis, Antonio Luna

ORCID number: Jordi Broncano (0000-0002-0683-8061); Ana María Alvarado-Benavides (0000-0003-1856-0690); Sanjeev Bhalla (0000-0002-1262-8925); Antonio Álvarez-Kindelan (0000-0003-1531-9543); Constantine A Raptis (0000-0003-0924-2447); Antonio Luna (0000-0001-9358-3396).

Author contributions: All authors contributed to this article.

Conflict-of-interest statement: There is no conflict of interest associated with any of the senior author or other coauthors contributed their efforts in this manuscript.

Manuscript source: Invited manuscript

Received: November 21, 2018
Peer-review started: November 23, 2018
First decision: December 10, 2018

Jordi Broncano, Cardiothoracic Imaging Unit, Hospital San Juan de Dios, Health Time, Cordoba 14012, Spain

Ana María Alvarado-Benavides, Sanjeev Bhalla, Constantine A Raptis, Cardiothoracic Department, Mallinckrodt Institute of Radiology, Washington University in Saint Louis, Saint Louis, MO 63110, United States

Antonio Álvarez-Kindelan, Thoracic Surgery Department, Hospital Reina Sofía, Cordoba 14004, Spain

Antonio Luna, MR imaging Unit, Clínica Las Nieves, Jaen 23007, Spain

Corresponding author: Jordi Broncano, MD, Staff Physician, Cardiothoracic Imaging Unit, Hospital San Juan de Dios, Health Time, Avenida el Brillante, 106, Cordoba 14012, Spain.
jordibroncano@gmail.com
Telephone: +34-957277000
Fax: +34-957277179

Abstract

In the new era of functional magnetic resonance imaging (MRI), the utility of chest MRI is increasing exponentially due to several advances, including absence of ionizing radiation, excellent tissue contrast and high capability for lesion characterization and treatment monitoring. The application of several of these diagnostic weapons in a multiparametric fashion enables to better characterize thymic epithelial tumors and other mediastinal tumoral lesions, accurate assessment of the invasion of adjacent structures and detection of pathologic lymph nodes and metastasis. Also, "do not touch lesions" could be identified with the associated impact in the management of those patients. One of the hot-spots of the multiparametric chest MR is its ability to detect with acuity early response to treatment in patients with mediastinal malignant neoplasms. This has been related with higher rates of overall survival and progression free survival. Therefore, in this review we will analyze the current functional imaging techniques available (^{18}F-Fluorodeoxiglucose positron emission tomography/computed tomography, diffusion-weighted imaging, dynamic contrast-enhanced MRI, diffusion tensor imaging and MR spectroscopy) for the evaluation of mediastinal lesions, with a focus in their correct acquisition and post-processing. Also, to review the clinical applications of these techniques in the diagnostic approach of benign and malignant conditions of the mediastinum.

Revised: February 28, 2019
Accepted: March 12, 2019
Article in press: March 12, 2019
Published online: March 28, 2019

P-Reviewer: Battal B, Kumar J, Xiao EH, Yang L
S-Editor: Yan JP
L-Editor: A
E-Editor: Wu YXJ

Key words: Mediastinum; Magnetic resonance; Diffusion; Perfusion; ^{18}F-Fluorodeoxiglucose positron emission tomography/computed tomography; Advanced imaging

Core tip: With the past improvements on magnetic resonance hardware, gradients and advanced sequences, the interest of magnetic resonance application in the chest is exponentially growing. In this review, we show the evidence in the literature of its application in mediastinal malignancies. In addition, we explore the advantages of applying new imaging techniques for lesion characterization, helping to differentiate with acuity benign and malignant etiologies. The use of several advanced sequences together yields specificity in identifying false positives from ^{18}F-Fluorodeoxiglucose positron emission tomography/computed tomography. Also, due to its precision in defining invasion and variation in tissue properties through the time, magnetic resonance enhances accurate staging and treatment monitoring.

Citation: Broncano J, Alvarado-Benavides AM, Bhalla S, Álvarez-Kindelan A, Raptis CA, Luna A. Role of advanced magnetic resonance imaging in the assessment of malignancies of the mediastinum. *World J Radiol* 2019; 11(3): 27-45
URL: https://www.wjgnet.com/1949-8470/full/v11/i3/27.htm
DOI: https://dx.doi.org/10.4329/wjr.v11.i3.27

INTRODUCTION

Morphological evaluation of mediastinal tumors are traditionally performed using computed tomography (CT). Magnetic resonance (MR) is considered a second-line test. However, other imaging methods are used to study tumor ultrastructure characteristics. Of them, the most validated and widely used is ^{18}F-Fluorodeoxiglucose positron emission tomography/CT (^{18}F-FDG-PET/CT) for assessing cell metabolism. Functional MR sequences, such as diffusion-weighted imaging (DWI) and perfusion-weighted imaging (PWI), are gradually becoming more available in daily clinical practice for assessment of mediastinal tumors. In addition to the absence of ionizing radiation, one of its significant advantages is the possibility of studying several physiological characteristics of tumors in the same protocol. Therefore, although technically very demanding, chest MR imaging (MRI) allows an integral evaluation of tumor and accurate differentiation from the non-neoplastic tissue.

Although there is scarce evidence in the literature, DWI helps to differentiate non tumoral thymic entities from thymo-epithelial neoplasms[1-3]. Moreover, by means of apparent diffusion coefficient (ADC) values, it could identify well-differentiated from more aggressive thymomas. DWI has a great value in the diagnosis, characterization and staging of central lung cancer and lymphoma[4]. Also, helps to characterize thyroid nodules and neurogenic tumors. By contrast, PWI is useful to characterize anterior mediastinal neoplasms. When a threshold time to peak of more than 120 seconds is used, it could separate non-invasive thymomas from invasive thymo-epithelial tumors, lymphoma and germ cell neoplasms[5]. The combination of DWI and PWI has demonstrated and increased in the diagnostic performance of MR in lung neoplasms[6]. Also, increases the precision of lung cancer staging by means of better identification of local invasion, metastatic lymph nodes (LN) and distant metastasis. By acquiring PWI and real time steady state free precession real time cine sequences (RT-SSFP), a higher conspicuity of mediastinal, pleural, chest wall and diaphragmatic invasion is obtained[7]. Finally, current data suggests a promising role of functional MRI in treatment monitoring of some neoplasms, like lung and esophageal cancer. The identification of early response has been liked to higher overall and progression free survival rates[8].

IMAGING TECHNIQUES AND OPTIMIZATION

Different imaging methods can study several tumor ultrastructure characteristics. The most widely available and validated molecular method is ^{18}F-FDG-PET/CT for

evaluating mainly, but not only, tumor glucose metabolism. Using other radiotracers, hypoxia and proliferation of mediastinal tumors, as long as the total tumor burden, could be analyzed. Recently, chest MR has become more widely available, allowing the assessment of different functional and morphological neoplastic characteristics in a one – stop – shop examination, with the advantage of avoiding the use of ionizing radiation.

Diffusion-weighted imaging

DWI interrogates the Brownian motion of water molecules of the tissues and lesions, particularly in the extracellular-extravascular space. DWI is a consolidated oncological biomarker in clinical practice, indirectly representing the occupancy of the interstitial space. For that purpose, several motion probe gradients are placed surrounding a 180° radiofrequency pulse. At least, two *b* values are necessary for analyzing the signal intensity decay of the tissues and calculating its ADC, following a mono-exponential model of diffusion signal decay[9]. In this manner, the higher the magnitude of signal intensity decay, the higher the ADC would be, indicating no restriction of water molecules. But, when a tissue shows restricted movement of water molecules, the signal intensity decay is lower and, therefore, ADC has a smaller value[10].

Intra-voxel incoherent motion (IVIM) model of diffusion signal decay is better than mono-exponential analysis for assessment of well-vascularized organs such as kidney, liver, pancreas, and prostate. For this model, it is necessary to acquire several b values. The diffusion signal decay splits into two components. At low *b* values (< 100-150 s/mm^2) the slope of signal decay is higher due to the bulk motion of water molecules inside randomly oriented capillaries (perfusion related decay of diffusion signal). But at higher *b* values (> 150 s/mm^2) the diffusion signal decay curve is related to the true diffusion of water molecules inside the tissue being evaluated (Figure 1)[9].

At very high *b* values (*b* > 1500 s/mm^2), there is a deviation of the theoretically mono-exponential based signal decay of DWI, that does not follow any Gaussian distribution. Diffusion kurtosis imaging explains this decreased slope of signal decay following a non–Gaussian distribution and relates it to tissue heterogeneity (Figure 1). In addition, these advanced models of quantification of DWI provide several derived parameters (Table 1).

Some cellular structures impede the diffusion of water molecules in one preferential direction. By the application of at least 6 non-collinear DWI gradients, a 3D diffusion profile of motion of water molecules could be plotted (diffusion tensor model) at a given voxel, which is an ellipsoid[11]. Therefore, when water molecules in a specified tissue move freely in all directions, the diffusion is isotropic. Contrarily, when this motion occurs mainly in one axis or axes due to structural properties of the tissue, this diffusion is anisotropic. Two metric measurements are derived. Mean diffusivity constitute the average diffusion in all three directions. Fractional anisotropy (FA) measures the degree of non-uniform diffusion in the three orthogonal directions[12].

Perfusion-weighted imaging

Tumor angiogenesis is essential for the development and behavior of solid tumors. Vasculature formation, growth patterns and vascular permeability are affected by antiangiogenic factors. Therefore, they modulate host response and weights tumor invasion, metastasis and outcome[13]. PWI is a functional technique focused on the evaluation of tumor neoangiogenesis[14,15]. It is a non-invasive and sensitive technique to neoplastic perfusion parameters such as blood volume, blood flow and vascular permeability[16].

There are two main technical approaches in the evaluation of tumor perfusion with MRI. Dynamic contrast-enhanced MRI (DCE-MRI) uses 2D or 3D gradient echo dynamic acquisitions, acquired during breath-holding. The temporal resolution of each dynamic acquisition is low (13-15 s), but with an excellent spatial resolution. Contrarily, PWI is based on ultrafast (2 to 3 s) 2D or 3D gradient echo dynamic sequences acquired during free-breathing. In order to achieve this very high temporal resolution, it is necessary to employ acceleration techniques such as non-Cartesian parallel imaging and compressed sensing, with the shortest available echo time[17]. Both of them show limited coverage, being higher in DCE-MR compared to PWI. Movement and respiratory artifacts are significant limitations of these techniques requiring the use of motion correction during post-processing[14]. Subtraction images are useful for adjacent structures infiltration detection. Semi-quantitative analysis can be performed with both types of acquisition, which benefits of the use of parametric color-coded maps. Because, these sequences track the variation of signal intensity secondary to gadolinium infusion per second, time-intensity curves (TIC) could be

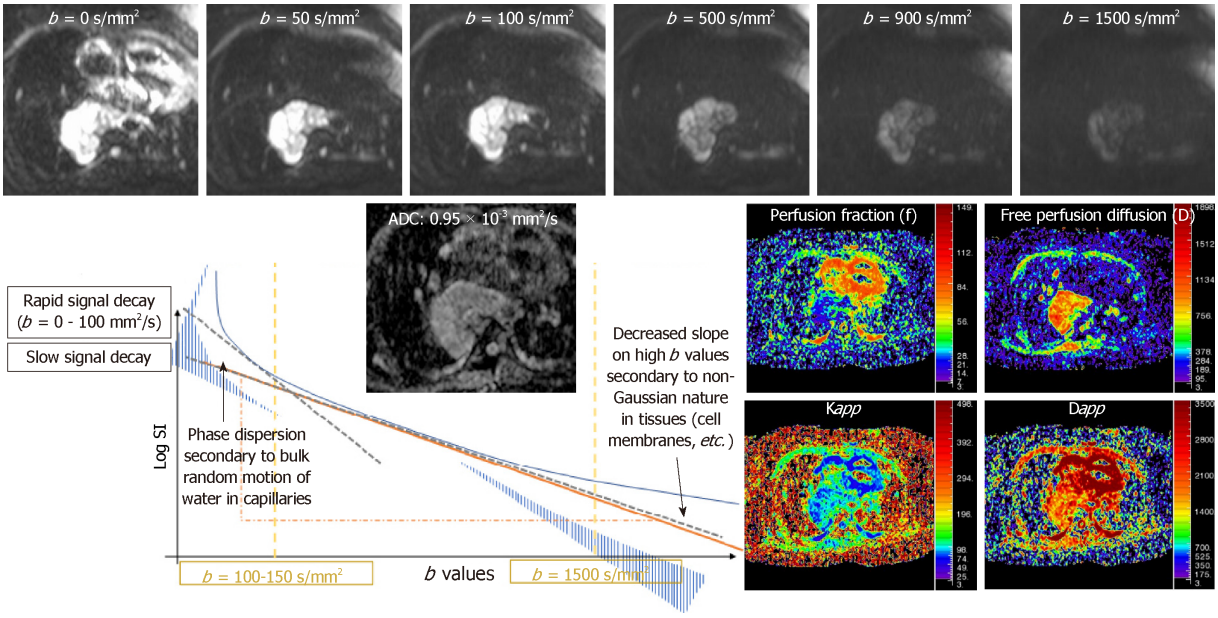

Figure 1 Different schemes on diffusion weighted imaging. Diagram represents the different diffusion weighted imaging models: Monoexponential, intravoxel incoherent motion and diffusion kurtosis imaging. Top images represent the behaviour of an esophageal leiomyosarcoma with different *b* values. Apparent diffusion coefficient and parametric maps of intravoxel incoherent motion -derived (perfusion fraction and free perfusion diffusion) and kurtosis-derived (K*app* and D*app*) biomarkers are also shown. IVIM: Intravoxel incoherent motion.

plotted (Figure 2).

PWI has the advantage to allow quantitative analysis using a mono-compartmental or bicompartmental approach. The mono-compartmental approach does not distinguish the intravascular and extravascular–extracellular compartments. Conversely, in the bicompartmental model, both spaces and the exchange of contrast agent between both of them are explored. For its quantification, a region of interest is placed in a principal artery, so the arterial input function is calculated. Additionally, it is possible to differentiate the transfer rates between both compartments. Mono and bicompartmental derived parameters are useful in tissue characterization and lesion management, and some of them have also demonstrated to be prognostic biomarkers of chest malignancies (Table 2)[16].

Other functional MR based techniques

Proton-based MR spectroscopy helps to depict the mi-croscopic metabolic microenvironment of tissues and lesions. The presence of a choline peak has been related to excessive cellular turnover in tumors outside the brain, helping to differentiate benign from malignant lesions[18]. To the best of our knowledge, there is no evidence in the literature about its utility in mediastinal tumors.

Blood oxygen level dependent imaging (BOLD) evaluates changes in the concentration of paramagnetic molecules, being a surrogate marker of tumor hypoxia, a well-known cause of radioresistance of malignancies. BOLD acquisition is based on a multi-echoT2*GE sequence, which is able to depict small reductions in T2* relaxation in tissues, secondary to increases in deoxyhemoglobin content during physiological gaseous exchange. Both, hyperoxia or hypercapnia challenges can be applied to depict changes in oxygen content within the tissues. Tissues with rising oxygen consumption would decrease T2* in those sequences. The rate of spin dephasing (R2* = 1/T2*) is related to the index of tissular oxygenation. Therefore, hypoxic tumors with high blood volume will show greater ΔR2* to physiological changes being, as a consequence, are less suitable to radiotherapy treatment[19].

ASSESSMENT OF MEDIASTINAL MASSES

The mediastinum is a complex segment of the chest, since it contains multiple vital structures in a reduced space. Traditional classification schemes have divided the mediastinum into three or four compartments. The 3-compartment models describe anterior, middle, and posterior divisions, and most 4-compartment models include superior, anterior, middle, and posterior divisions. The International Thymic Malignancy Interest Group (ITMIG) propose a 3-compartment model of the

Table 1 Diffusion weighted derived parameters of different model analysis

Mono-exponential model		
ADC	Apparent diffusion coefficient	Exponential signal decay of water molecules in a voxel by voxel basis.
IVIM-derived parameters		
D	True diffusion of H_2O molecules	Not influenced by movement of water molecules within capillaries
f	Perfusion contribution to diffusion signal	Fractional volume of flowing water molecules within capillaries
D	Perfusion contribution to diffusion signal decay	Amount of non-diffusional random movements of water molecules
DKI-derived parameters		
D*app*	Apparent diffusion	Estimation of diffusion coefficient in the direction parallel to the orientation of diffusion sensitizing agents
K*app*	Apparent diffusional kurtosis	Measures the deviation of the true diffusion from a Gaussian pattern.
DTI-derived parameters		
MD	Mean diffusivity	Reflects the average diffusion of water molecules in all three directions.
FA	Fractional anisotropy	Measures the extent to which diffusion is non-uniform in the three orthogonal directions.

ADC: Apparent diffusion coefficient; IVIM: Intravoxel incoherent motion; MD: Mean diffusivity; FA: Fractional anisotropy.

mediastinum based on boundaries identifiable on routine cross-sectional imaging. These segments include prevascular (anterior), visceral (middle), and paravertebral (posterior) compartments[20].

Prevascular (anterior) mediastinal lesions

Thymic hyperplasia: Thymic hyperplasia manifests as diffuse symmetric enlargement of the thymus. There are two histologic types of thymic hyperplasia: lymphofollicular hyperplasia and true thymic hyperplasia. Lymphofollicular hyperplasia refers to the presence of hyperplastic lymphoid germinal centers with lymphocytic and plasma cell infiltrate. It is most commonly associated with myasthenia gravis (50% of patients) and other autoimmune conditions such as thyrotoxicosis, systemic lupus erythematosus (SLE), rheumatoid arthritis, scleroderma, among others. True thymic hyperplasia is an enlargement of the thymus, without histologic abnormalities. Rebound hyperplasia occurs after chemotherapy, steroids, and radiotherapy[21].

In patients with diffuse thymic enlargement, it may be difficult to differentiate between hyperplasia and tumor. Fat infiltration is present within the normal thymus and thymic hyperplasia[22]. Chemical shift imaging (CSI) is a fat-suppression technique that enables the identification of microscopic or intravoxel fat[1]. It allows the detection of an intravoxel mixture of water and fat by showing a signal loss on the opposed-phase image relative to the in-phase image in the thymic tissue compared to paraspinal muscle. CSI can be used to distinguish thymo-epithelial tumor from thymic hyperplasia, by detecting microscopic fat in the latter. A chemical shift ratio (CSR) can be calculated for quantifying the signal suppression on opposed-phase divided by the signal intensity in-phase of the thymic tissue related to the paraspinal muscle. A CSR value of less than or equal to 0.7 is suggestive of thymic hyperplasia, depending on sex and age[23]. When the CSR is over 1.0, it is indicative of tumoral origin. Between 0.8 and 0.9 the lesion is unclear and a control examination is needed. It is essential to take into account that not all young thymus suppress fat in out of phase imaging[24]. Also, the thymus of young women had lower CSR than the thymus of young men[25]. On DWI, thymic hyperplasia shows no significant restriction of free water molecules, revealing higher ADC values compared to tumoral lesions. Also, on DCE-MRI, it shows minimal (type D) or no enhancement after gadolinium intake. Meanwhile, thymic tumors show increased perfusion.

Thymic epithelial neoplasms: Thymic epithelial neoplasms are rare malignant tumors, with a described prevalence of 0.13/100000 individual in the United States[3]. Thymic epithelial neoplasms include thymoma, thymic neuroendocrine tumors (NETs), and thymic carcinoma. Up to 15 different staging systems have been

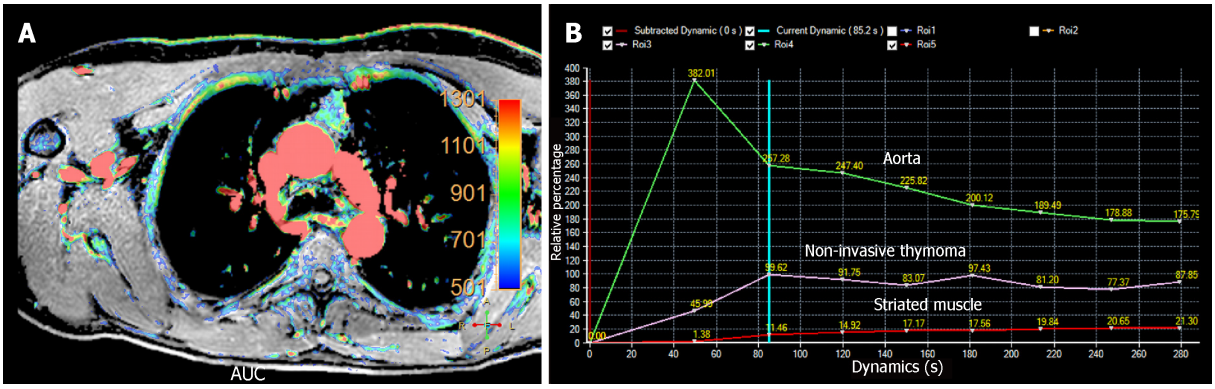

Figure 2 Perfusion weighted imaging of non-invasive thymoma. A 38 year - old male with an anterior mediastinal well-defined solid nodule, without signs of local infiltration of adjacent structures. A: Dynamic contrast-enhanced magnetic resonance (DCE-MR) derived area under the curve parametric map reveals a significant uptake of intravenous gadolinium based contrast (white arrow); B: DCE-MR derived time intensity curve shows a moderate initial slope of enhancement with a delayed plateau and with a time to peak less than 120 s (pink curve). This is in keeping with non–invasive thymoma (stage I Masaoka–Koga). AUC: Area under the curve; DCE-MR: Dynamic contrast-enhanced magnetic resonance.

described for thymo-epithelial neoplasms. The Masaoka system and its variant, the Masaoka–Koga staging system, are the most commonly used in clinical practice (Table 3). The radiologist has a crucial role in the staging, because the identification of advanced stages (III and IV) directs the patient towards neoadjuvant therapy[2]. In fact, the ITMIG recommended this staging system due to its correlation with patient survival[26]. Recently, the ITMIG in association with the International Association for the Study of Lung Cancer proposed a TNM staging system according to conclusions obtained from the retrospective inclusion of more than 10000 patients (Table 4)[27].

Thymoma is the most common histologic type of thymic epithelial neoplasms of the prevascular mediastinum. Men and women are affected equally. Has a peak incidence in middle age (40-60 years) and is rare in children and young adults[2]. About 20% of thymomas coexist with other neoplasms such as lymphoma, lung cancer, and thyroid cancer. Thymomas are slow-growing neoplasms and, although an aggressive behavior is rare, they may present pleural, pericardial, and more unusually, hematogenous spread[28]. The association of thymoma with myasthenia gravis is common. Between 30 to 50% of thymomas coexist with myasthenia gravis, being more frequent this relation in women, and up to 10% to 15% of patients with myasthenia gravis have a thymoma[1,2]. Other associated conditions are hypogammaglobulinemia (10%), pure red cell aplasia (5%), Good's syndrome (B and T cell immunodeficiency) and autoimmune disorders (SLE, polymyositis, and myocarditis)[29].

On MRI, thymomas have low to intermediate signal intensity on T1 and high signal intensity on T2-weighted sequences. They may present with cystic changes, necrosis, fibrous septa, nodules, and hemorrhage[4]. DWI is useful for differentiating between benign and malignant tumors by using ADC values. The study by Razek *et al*[4] showed ADC values of 2.38 ± 0.65 × 10^{-3} mm^2/s and 1.09 ± 0.25 × 10^{-3} mm^2/s, for benign and malignant tumors. They defined a threshold ADC value of 1.56 × 10^{-3} mm^2/s for differentiating malignant from benign mediastinal neoplasms, with a sensitivity, specificity, and accuracy of 96%, 94%, and 95%, respectively. Additionally, well-differentiated tumors showed higher ADC values (1.20 ± 0.22 × 10^{-3} mm^2/s) compared to poor differentiated tumors (0.98 ± 0.18 × 10^{-3} mm^2/s). Nevertheless, there was an overlap in the ADC values of invasive thymoma, lymphoma and lung cancer. Consequently, the solely use of ADC values cannot differentiate them with accuracy[4]. On the other hand, Yabuuchi *et al*[5] found no significant difference in ADC values between thymic epithelial tumors, lymphomas and malignant germ cell tumors. Furthermore, Carter *et al*[3] stated that ADC could not differentiate between low-grade thymomas, high-grade thymomas and thymic carcinomas.

DCE-MRI can be used to differentiate anterior mediastinal masses. Yabuuchi *et al*[5] described 3 types of time-signal intensity curves: (1) Persistent, with a time-to-peak (TTP) > 120 s; (2) Plateau, with a TTP < 120 s and a wash-out < 30%; and (3) Wash-out, with a TTP < 120 s and wash-out > 30%. In their population, the washout pattern was seen only in thymic epithelial tumors (Figure 2). Also, they added the use of ^{18}FDG-PET for this differentiation. The combination of TIC pattern (washout or persistent/plateau pattern), maximal diameter (< 6.8 cm *vs* ≥ 6.8 cm), and a maximum standardized uptake value (SUV_{max}) cut off value of 11.6 could help differentiate between thymoma (SUV_{max} < 11.6) and thymic carcinoma (SUV_{max} > 11.6). They proposed a flow diagram combining the TIC pattern, SUV_{max}, and maximal diameter

Table 2 Perfusion weighted imaging derived parameters

Semiquantitative parameters	
Initial area under the curve	Include information of blood flow, blood volume, permeability, extravascular–extracellular space volume and microvessel density.
Time to peak	Depends on tissue perfusion
Wash in	Represents velocity of enhancement
Wash out	Represents velocity of enhancement loss
Quantitative parameters	
K^{trans}	Influx volume transfer constant of a contrast agent from the vascular compartment to the interstitial space
V_e	Volume of extravascular–extracellular space per unit of tumor volume
V_p	Blood plasma volume
K^{ep}	Rate constant between extravascular-extracelular space and plasma

for characterization of anterior mediastinal solid tumors. With this scheme, they obtained a sensitivity and specificity of 93.9% and 77.8%, respectively, for differentiating anterior mediastinal tumors (Figure 3)[5].

On the other hand, Sakai *et al*[30] found a correlation between histologic grade and DCE-MRI parameters. Low-risk thymomas (Masaoka stage I/II) demonstrated rapid TTP with a mean time of 1.5 min; Masaoka stage III showed a TTP of 2.5 minutes, and other lesions such as thymic carcinoma, NETs, lymphoma, and malignant germ cell tumor demonstrated progressive enhancement, with a TTP of 3.2 min. The differentiation of thymoma from other mediastinal masses showed a sensitivity, specificity, and accuracy of 79%, 84%, and 81% respectively, when a cut-off value of TTP < 2 min was used (Figure 4).

NETs or thymic carcinoid are the least common type of thymic epithelial neoplasms (incidence 525 cases per 100000 people per year in the United States)[31]. Thymic NETs primarily affect males (male to female ratio of 3:1) in their sixth decade of life. The median age at presentation is approximately 57 years. Thymic NETs originate from neural crest cells and are associated with poor prognosis as they are aggressive, locally invasive with distant metastases and resistant to chemotherapy[32]. Nearly 25% of thymic NETs arise in patients with multiple endocrine neoplasia type 1, Cushing syndrome and inappropriate antidiuretic hormone secretion syndrome[33].

Imaging findings are similar to those of thymomas at CT and conventional MR, although, they tend to be larger, lobulated and locally invasive masses. As well as thymic carcinomas, suggestive findings include: (1) Irregular contour and cystic component; (2) metastasis and vascular invasion; and (3) heterogeneous enhancement and lymphadenopathy. They may present with low ADC values, which represents aggressiveness, hypercellularity, and poor differentiation. Additionally, a DCE-MRI with a TTP > 2 min suggests a high-grade tumor[4,5,30].

Thymic carcinomas are the second most common type of thymic epithelial neoplasms, representing up to 20% of those tumors[34]. Middle age men are more commonly affected. Thymic carcinomas are more aggressive and invasive than thymomas, with a larger size, lobulated contour, and invasion of adjacent structures. They may also present with cystic changes and necrosis. Poor prognosis is related with infiltrating tumor margin, the absence of a lobular growth pattern, high-grade atypia and necrosis, and more than ten mitoses per High-Power Field[35,36].

Thymic carcinomas present similar findings at CT and conventional MR as thymomas. Suggestive signs of thymic carcinomas are the presence of metastases, vascular invasion, irregular contour, cystic component, heterogeneous enhancement, and lymphadenopathy[35,36]. As well as thymic NETs, low ADC values suggest aggressiveness and poor differentiation, and DCE-MRI with a TTP > 2 min indicates a high-grade tumor (Figure 3). High ^{18}FDG uptake is another characteristic that may help differentiate between thymoma and thymic carcinoma, with the latter presenting with higher SUV_{max} values (Figure 4)[4,5,30].

Lymphoma: Lymphoma comprises a heterogeneous group of neoplasms involving the LN. Mediastinal involvement is frequently a part of the systemic disease. Primary mediastinal lymphomas are rare (10%). The majority of lymphomas affecting the mediastinum are Hodgkin lymphoma (HL)[37]. There were 66000 new cases of non-Hodgkin lymphoma (NHL) and 8800 new cases of HL diagnosed in the United States in 2011[38-40]. The value of imaging techniques relies on the capacity to differentiate reactive from malignant lymph node, but also to evaluate tumor extension, treatment

Table 3 Masaoka–Koga staging system

Stage	Degree of invasion	5 yr survival rate (%)
I	Tumor completely encapsulated	96-100
IIa	Microscopic tumor invasion into the capsule	86-95
IIb	Tumor invasion into the surrounding fat	
III	Tumor invasion into surrounding organ such as the pericardium, great vessel or lung	56-69
IVa	Pleural or pericardial dissemination	11-50
IVb	Lymphatic or hematogeneous metastasis	

response, and relapse. Additionally, the ability to discriminate lymphoma subtypes allows treatment assessment, outcome, and differentiation between indolent and aggressive NHL[41].

It usually presents as an anterior mediastinal soft-tissue mass or a conglomerate of LN with mild enhancement. The association of lymphadenopathy affecting different lymph node stations in the chest without mediastinal mass suggests a secondary involvement of NHL arising from other location[27]. When a mediastinal mass shows an infiltrative nature with encasement or encirclement of vascular structures without involving it, a lymphoma should be the first entity to keep in mind over thymo-epithelial or germ cell tumors[27].

^{18}FDG-PET/CT is better than ^{18}FDG-PET or CT alone for evaluating lymphoma as it helps to discriminate indolent from aggressive NHL. In 2016, the International Workshop on NHL approved the new response evaluation criteria in lymphoma (RECIL). RECIL criteria are aligned with response evaluation criteria in solid tumors, in as much as it suggests a uni-dimensional measurement method, but introduce tumor metabolic evaluation with ^{18}FDG-PET/CT. SUV_{max} is useful for evaluating treatment response and outcome in ^{18}FDG-avid lymphoma. There is an excellent correlation between high SUV_{mean} values and progression-free survival (PFS)[42].

DWI reveals inherent tissue properties, such as hypercellularity, nuclear hyperchromatism and an increase in the number of macromolecular proteins. Koşucu *et al*[43] described the utility of ADC values in the differentiation of malignant and benign mediastinal LN. They found the lowest ADC values in metastatic LN compared to benign LN ($1.02 \pm 0.19 \times 10^{-3}$ mm^2/s *vs* $1.51 \pm 0.07 \times 10^{-3}$ mm^2/s, for malignant and benign LN respectively). Also, an overlap in ADC values was present with invasive thymoma and bronchogenic carcinoma. The study by Mosavi *et al*[44] showed a difference in ADC values between indolent NHL, aggressive NHL and HL using whole-body DWI, with ADC values being lower in indolent NHL (597 ± 115 mm^2/s) rather than aggressive NHL (822 ± 266 mm^2/s) and HL (1020 ± 547 mm^2/s) (Figure 5). The explanation for lower values of ADC in indolent NHL could be explained by the higher cell density when compared to HL and aggressive NHL. Additionally, an increased ADC value has been related to longer overall survival (OS). Whole body DWI had a similar diagnostic performance to ^{18}FDG-^{18}FDG-PET/CT. Therefore, in the assessment of early treatment response, usually at after one week, could be an alternative radiation-free surveillance method. PET/MR could be a promising alternative method for staging and follow up of patients with lymphoma. In fact, ADCs and SUVs demonstrate to be independent biomarkers in lymphoma, with significant correlation between them in follicular lymphoma[17].

Germ cell tumors: They comprise neoplasms arising from primitive germ cells, miss-migrated along the urogenital ridge. There are two types, of seminomatous (seminoma and dysgerminoma) or non-seminomatous (NSGCT) origin (embryonal carcinoma, choriocarcinoma, Yolk-Salk tumor, and teratoma). Malignant germ cell tumors usually have a male predominance. Mature teratoma constitutes the most common mediastinal germ cell tumor, demostrating a varying amount of intralesional fluid, fat (present in up to 50% of cases), calcification or soft tissue components. Frequently, teratomas manifest as large unilocular or multilocular thin-walled cystic masses[3]. Occasionally, bones or tooth-like elements could be identified[45,46]. Fat-fluid levels are highly specific to this entity, which typically affect young patients, with a described prevalence of 25% of the prevascular masses in patients of 10-19 years-old, 10%-15% in individuals of 20-49 years old and less than 5% in subjects of more than 50 years-old[47]. Differential diagnosis includes other fat-containing anterior mediastinal lesions like thymolipoma, lipoma or liposarcoma.

Non-teratomatous germ cell tumors usually manifest as large soft-tissue prevascular mediastinal masses. Clinical and serological information is useful in the

Table 4 The tumor node metastasis staging system by International Thymic Malignancy Interest Group

		TNM staging					
Tumor (T) descriptor		**I**	**II**	**IIIA**	**IIIB**	**IVA**	**IVB**
T1a	Encapsulated or unencapsulated tumor, with or without extension into fat	X				X	X
T1b	Invasion of mediastinal pleura	X				X	X
T2	Invasion of pericardium		X			X	X
T3	Involvement of lung, chest wall, phrenic nerve, brachiocephalic vein, superior vena cava, or hilar (extrapericardial) pulmonary vessels			X		X	X
T4	Invasion of thoracic aorta, arch vessels, main pulmonary artery, trachea, esophagus, or myocardium				X	X	X
Node (N) descriptor		**I**	**II**	**IIIA**	**IIIB**	**IVA**	**IVB**
N0	No lymph node metastasis	X	X	X	X	X	X
N1	Involvement of anterior (perithymic) lymph nodes					X	X
N2	Involvement of deep intrathoracic or cervical lymph nodes						X
Metastasis (M) descriptor		**I**	**II**	**IIIA**	**IIIB**	**IVA**	**IVB**
M0	No Metastasis	X	X	X	X	X (N1)	X (N2)
M1a	Pleural or pericardial metastatic nodule or lesions					X (N0,1)	X (N2)
M1b	Pulmonary intraparenchymal metastastic nodule or distant organ metastasis						X (any T, N)

TNM: Tumor node metastasis staging system; ITMIG: International Thymic Malignancy Interest Group.

differentiation of these lesions with lymphoma. Seminomas generally affect patients between 10 to 39 years old. In up to 10% of patients, there is an elevation of serum levels of beta-human chorionic gonadotropin (b-HCG)[48]. Elevated levels of lactate dehydrogenase could be present in seminomas but also in lymphoma patients[49,50]. Contrarily, NSGCT present with high levels of serum b-HCG and alpha-fetoprotein in 90% of them[51,52]. Seminomatous tumors manifest as hypointense masses on T2-weighted images, with homogeneous enhancement after gadolinium uptake. By contrast, NSGCT are large and heterogeneous masses. Internal foci of hyperintensity on T1-weighted images are related to intralesional hemorrhage. Although, the presence of pleural effusion is rare, pulmonary metastasis may help to distinguish seminomatous germ cell tumors from lymphoma. An NSGCT is firstly suspected when a large and heterogeneous prevascular mass with pulmonary nodules is

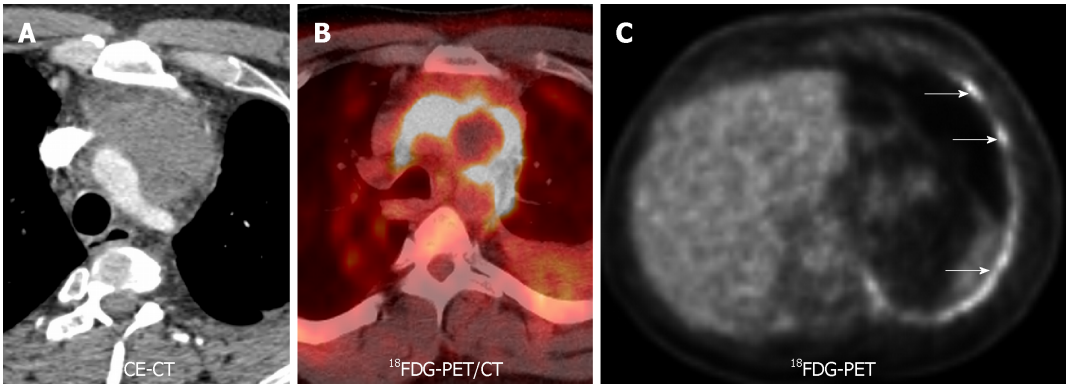

Figure 3 ^{18}F-Fluorodeoxiglucose positron emission tomography/computed tomography of a thymic carcinoma. A 34-year-old with chest pain, found to have infiltrative mass on pulmonary embolism protocol. Pathology revealed a thymic carcinoma. A and B: Contrast-enhanced computed tomography and fused ^{18}F-Fluorodeoxiglucose positron emission tomography/computed tomography showed an ^{18}F-Fluorodeoxiglucose avid anterior mediastinal mass infiltrating thoracic vascular vessels; C: Concentric increased ^{18}F-Fluorodeoxiglucose activity in the left pleura was proven to represent metastatic disease (white arrows). ^{18}F-FDG-PET/CT: ^{18}F-Fluorodeoxiglucose positron emission tomography/computed tomography; ^{18}FDG-PET: ^{18}F-Fluorodeoxiglucose positron emission tomography; CE-CT: Contrast-enhanced computed tomography.

identified on a male patient below 40 years-old[45,53]. DWI could help to differentiate a benign from a malignant origin, but also, may increase our specificity to detect mature fibrosis or cystic components. At DCE-MR, they usually show a persistent or plateau pattern of TIC, with a TTP over 120 s. On ^{18}FDG-PET/CT, they show a high radiotracer uptake, often with maximum SUVs higher than 11.6 (Figure 6). The combination of size, DCE-MR derived TIC, and ^{18}FDG-PET/CT along with serologic markers could help to differentiate germ cell tumors from other anterior mediastinal masses[5].

Mediastinal goiter: It has a described incidence of 1%-15% of patients undergoing thyroidectomy. On a CT exam, when a hyperattenuating (70-85 Hounsfield units) prevascular mediastinal mass with intense and sustained enhancement is identified in continuity with the cervical thyroid gland, a mediastinal goiter should be the most preferred diagnosis. Cystic changes and calcifications may be present. Additional findings favouring a malignant transformation are loss of mediastinal tissue planes and cervical or mediastinal lymphadenopathy[27,47].

DWI could help to differentiate benign from malignant thyroid nodules. Using a b value of 500 s/mm^2 and an ADC cut-off value of 1.704 × 10^{-3} mm^2/s, a sensitivity, specificity, and accuracy of 92%, 88%, and 87%, respectively has been described. Additionally, using a DW-sequence with a *b* value of 1000 s/mm^2, significant differences on ADC values have been described between benign and malignant nodules (2.75 ± 0.6 × 10^{-3} mm^2/s *vs* 0.69 ± 0.35 × 10^{-3} mm^2/s). The decrease in ADC values in malignant lesions is due to the presence of increased cell density and relatively severe desmoplastic response. Contrarily, the cause of elevated ADC in thyroid adenomas and hyperplastic nodular goiter is the predominance of abundant cellular follicles, extracellular fluid and reduced cell density[54]. Furthermore, the presence of a delayed wash-out pattern is also suggestive of thyroid carcinoma, with higher diagnostic performance compared to fine needle aspiration (sensitivity 100% *vs* 50%-85.7%; accuracy 90% *vs* 70% to 87.5%, respectively)[55].

Parathyroid adenoma: It usually presents in a patient with a history of primary hyperparathyroidism, hypercalcemia and/or elevated serum parathormone levels, with or without parathyrodectomy and a soft-tissue nodule in the anterior–prevascular mediastinum[56]. 20% of parathyroid adenomas are ectopic, and 80% of ectopic parathyroid adenomas showed an anterior mediastinal location. Possible ectopic locations include the thymus, tracheoesophageal groove, retrosternal region and posterosuperior mediastinum[36]. On imaging, they usually present as small (< 3 cm) rounded and well-defined nodules, with high radiotracer uptake at ^{99m}Tecnetium and ^{201}Talium scans[27]. Four dimensional (4D) CT provides both functional (perfusion) and highly detailed anatomic knowledge about parathyroid lesions. At 4D CT imaging, they present strong enhancement after intravenous contrast infusion with significant washout at the delayed phase[57,58]. Although there is no reference in the literature about the utility of DWI and DCE-MR in parathyroid adenoma, in the authors' experience, these lesions demonstrate high ADC values and, and on PWI, a TIC with a steep slope and significant washout, in a similar fashion to the findings described on 4D CT[27].

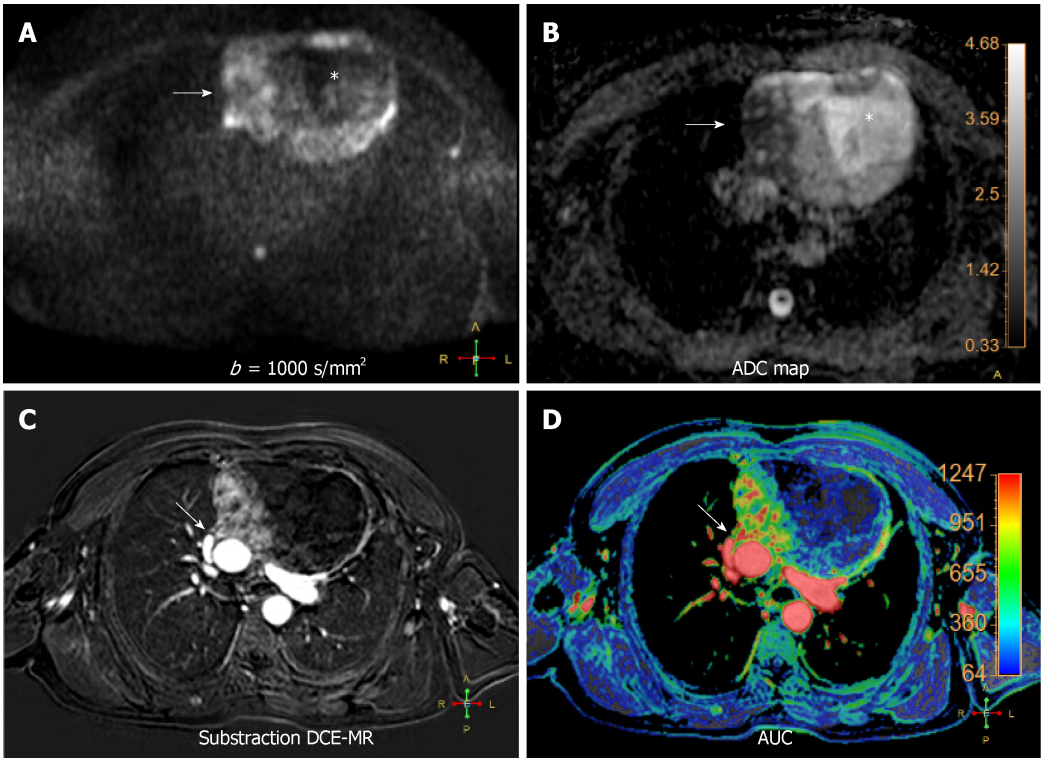

Figure 4 Multiparametric functional magnetic resonance imaging thymoepithelial mass. A 63 year-old male with a complex cystic anterior mediastinal mass. A and B: High *b* value diffusion-weighted imaging (DWI) (*b* = 1000 s/mm^2) (A) and corresponding apparent diffusion coefficient (ADC) map (B) revealing the complex behaviour of the lesion. In this case, DWI can differentiate the solid (white arrow on A and B) and cystic (white asterisk on A and B) components and also reveals heh restrictive behaviour of the solid part of the mass (ADC: 1.12-1.23 × 10^{-3} mm^2/s), related to hypercellularity; C and D: Substraction of dynamic contrast-enhanced magnetic resonance on the arterial phase (C) and area under the curve parametric map (D) showing the locally invasive behaviour of the lesion to the pericardium and adjacent ascending aorta (white arrows on C and D). The mass corresponded to an invasive thymoma stage III of Masaoka–Koga classification system. DWI: Diffusion-weighted imaging; ADC: Apparent diffusion coefficient; AUC: Area under the curve; DCE-MR: Dynamic contrast-enhanced magnetic resonance.

Visceral mediastinal lesions

Central lung cancer: Functional MR has shown great utility in patients with lung cancer, enabling to differentiate with accuracy benign from malignant nodules. The combination of DWI and DCE-MR showed similar sensitivity to ^{18}FDG-PET-CT but higher specificity and accuracy (up to 94%), thanks to the reduction of the number of false positives from the latter technique, such as active inflammatory and tuberculous nodules[6]. In addition, DWI has a potential impact on lung cancer differentiation. Well-differentiated adenocarcinomas display higher ADC values than aggressive adenocarcinomas, with certain overlap with small cell lung cancer and squamous cell lung cancer[59]. The amount of tumor cells and its distribution is related to signal intensity at high *b* value. A signal intensity lesion-to-spinal cord ratio (LSR) on high b value has been explored in the differentiation of malignant and benign ones. Malignant tumors demonstrated higher values, having more specificity and accuracy than ADC and IVIM derived values in this differentiation[60,61]. Furthermore, aggressive subtypes of adenocarcinoma showed higher signal intensity at high b value with a heterogeneous pattern. However, other authors did not show significant differences in the LSR of benign and malignant pulmonary lesions (Figure 7)[62].

Different patterns of enhancement have been described in primary mediastinal neoplasms, although some overlap is also present[63-66]. Some authors obtained higher relative signal enhancement and steeper slope in active inflammatory lesions[66]. Coolen *et al*[63] described a flowchart , where the use of DWI in lesions with TIC type B curves could distinguish benign (non-restrictive) from malignant (restrictive) entities (Figure 7). Therefore, functional multiparametric chest MRI constitutes a valuable one-stop-shop radiation-free diagnostic modality for lung cancer characterization.

Paravertebral mediastinal masses

Neurogenic tumors group a certain type of lesions that arise from peripheral nerves, sympathetic and parasympathetic ganglia. Correspond to 75% of all posterior mediastinal lesions, 20% of adult posterior mediastinal lesions and 25% of pediatric mediastinal lesions[3]. There are significant differences in the ADC of benign and malignant peripheral nerve tumors (1.848 ± 0.40 × 10^{-3} mm^2/s *vs* 0.900 ± 0.25 × 10^{-3}

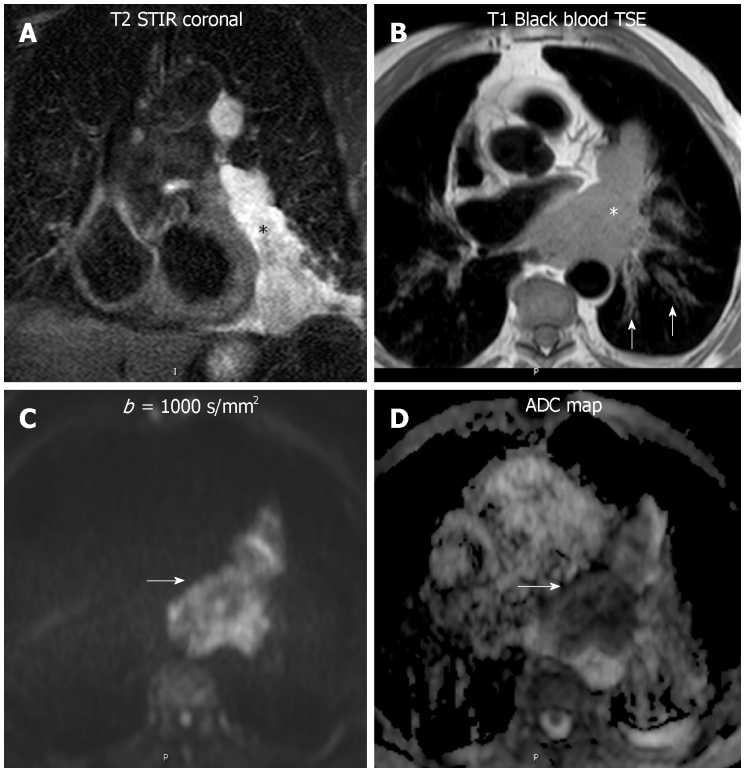

Figure 5 Diffusion weighted imaging of a lymphoma. An 82 year - old man with a paracardiac lymphomatous mass. A: The lesion is hyperintense in short tau inversion recovery (black asterisk); B: On black blood turbo spin echo T1-weighted image, the lesion is slightly hyperintense compared to striated muscle (white asterisk), with infiltration of the pericardium and hilar vessels. Secondary involvement of the left axial interstitium, bilaterally (white arrows on B); C and D: In high *b* value diffusion-weighted imaging (*b*: 1000 s/mm^2) the mass showed high signal intensity, with low apparent diffusion coefficient: 1.1 × 10^{-3} mm^2/s on the apparent diffusion coefficient map, in keeping with lymphoma (white arrows on C and D). STIR: Short tau inversion recovery; TSE: Turbo spin echo; ADC: Apparent diffusion coefficient.

mm^2/s; for benign and malignant tumors, respectively, $P < 0.001$)[67]. Also, the FA derived from diffusion tensor imaging of involved nerves was lower compared to normal ones[67]. There is limited evidence about the application of functional MRI in other mediastinal lesions.

FUNCTIONAL MR AND STAGING

Functional MR has shown great utility in the staging of lung cancer by allowing an accurate assessment of invasion of vascular, bronchial and other mediastinal and chest wall structures. DWI can differentiate, without the need for any radiotracer intake, central tumor (restrictive) from post-obstructive pneumonitis (non-restrictive), which is vital for cancer staging and radiotherapy planning. DCE-MR is superior to contrast enhanced CT and morphological MR in the identification of vascular and mediastinal invasion[12]. Free breathing RT-SSFP sequences can distinguish those peripheral tumors invading only the visceral pleura (mobile with respiratory motion) rather than those that invade parietal pleura and beyond (static with respiratory motion). Therefore, the combination of DCE-MR and RT-SSFP could be an optimized strategy for assessing pleural, mediastinal, diaphragmatic and chest wall invasion.

For nodal staging (N-staging) ^{18}FDG-PET/CT constitute the primary modality in lung cancer. The primary objective is to identify occult metastatic LN and distant lesions. It could discriminate N3 from M1 stages, which require neoadjuvant therapy. By contrast, DWI has also shown great utility in the differentiation of benign from malignant LN, distinguishing false positive ^{18}FDG-PET/CT targets due to reactive – inflammatory LN. In DWI, false positives are due to granulomatous LN, and false negatives are secondary to microscopic cancer deposits, mainly. Nomori *et al*[68] detected higher ADC values in benign lymph nodes compared to metastatic ones, using an ADC threshold value of 1.63 × 10^{-3} mm^2/s (accuracy: 89%, specificity: 99%). Finally, Chhabra *et al*[67] applied a semiquantitative approach. They referred that short tau inversion recovery was more sensitive and accurate for N staging compared to

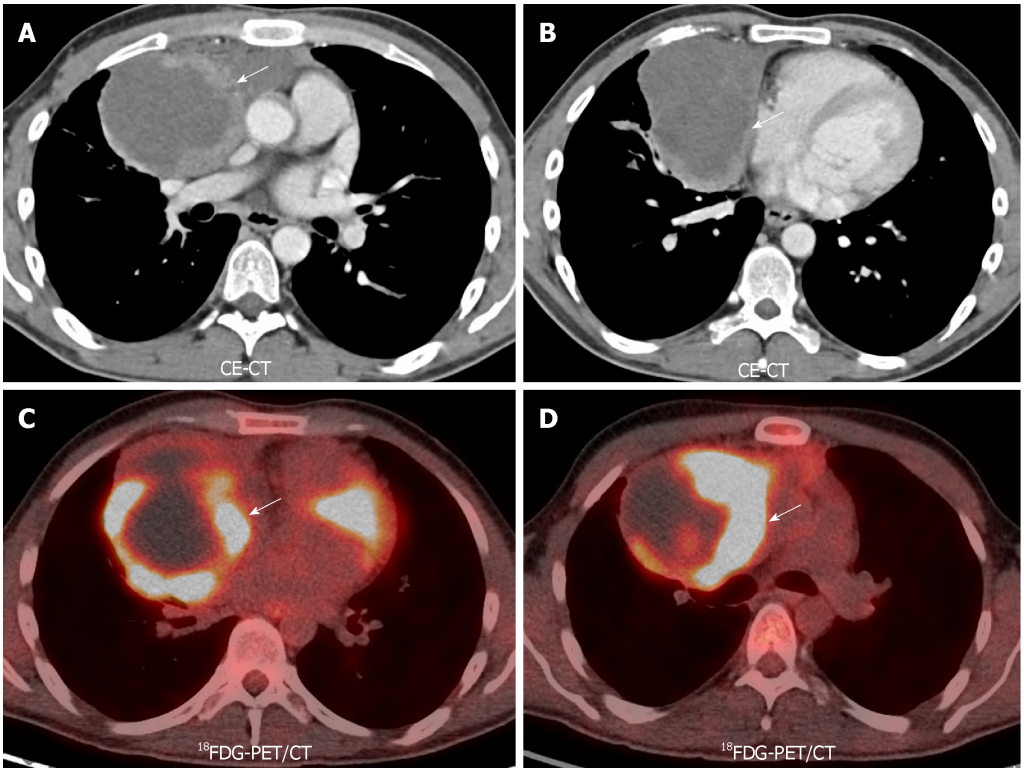

Figure 6 ^{18}F-Fluorodeoxiglucose positron emission tomography/computed tomography of a germ cell tumor. A 27-year-old man with back pain, found to have germ cell tumor on ^{18}F-Fluorodeoxiglucose positron emission tomography/computed tomography (^{18}FDG-PET/CT). A and B: Contrast-enhanced CT shows a cystic mass with enhancing solid border (white arrows on A and B); C and D: Note ^{18}FDG activity only within the solid portions of the lesion on fused ^{18}FDG-PET/CT acquisitions (white arrows on C-D). ^{18}FDG-PET/CT: ^{18}F-Fluorodeoxiglucose positron emission tomography/computed tomography; CE CT: Contrast-enhanced computed tomography.

DWI and ^{18}FDG-PET/CT.

^{18}FDG-PET/CT is the current standard technique for staging esophageal cancer, with an overall accuracy of 90%-92%. False negatives are due to early stage (T*in situ*, T1 and T2). False positives of this technique are secondary to leiomyomas and esophagitis (Figure 8). Another limitation is the poor spatial resolution, which explains its limited role in defining the depth of invasion. MRI has no role in current staging guidelines. MR also has poor detection rates in the early stages. The detection rates using a combination of high resolution T2 and DWI are 33%, 58%, 96% and 100% for T1, T2, T3, and T4 stages, respectively[69]. Contrarily to lung cancer LN, in esophageal carcinoma the ADC of malignant LN is higher than benign LN ($1.46 \pm 0.35 \times 10^{-3}$ mm^2/s *vs* $1.15 \pm 0.25 \times 10^{-3}$ mm^2/s, $P < 0.0001$), due to their mucinous content[70].

Whole body–DWI (WB-DWI) is a promising tool for M staging, which globally reflects similar results to ^{18}FDG-PET/CT. In detail, it is superior to bone scintigraphy, ^{18}FDG-PET/CT and CT in the identification of bone metastasis, and has substantial advantages in the detection of bone, liver, brain, and kidney metastasis[71]. Contrarily, compared to a WB-DWI scheme, ^{18}FDG-PET/CT has better results in LN and soft-tissue metastasis, probably due to the non-selective fat saturation technique applied for background signal suppression in WB-DWI[72,73].

CHEST MR IN EARLY RESPONSE AND TREATMENT MONITORING

One of the most promising applications of functional MR in the chest is treatment monitoring and detection of recurrence (Table 5). An increase in ADC in patients of non-small cell lung cancer during or after chemotherapy or radiotherapy has been related to good response, being associated to higher OS and PFS. This increase in ADC is due to cell death, necrosis, apoptosis, and cell lysis. DWI has better results for detection of early response than DCE-MR and ^{18}FDG-PET/CT. Also, a low ADC value at the pre-treatment stage has been predictive of proper response to chemotherapy[8,74,75].

Another important application of DWI is the treatment monitoring of new

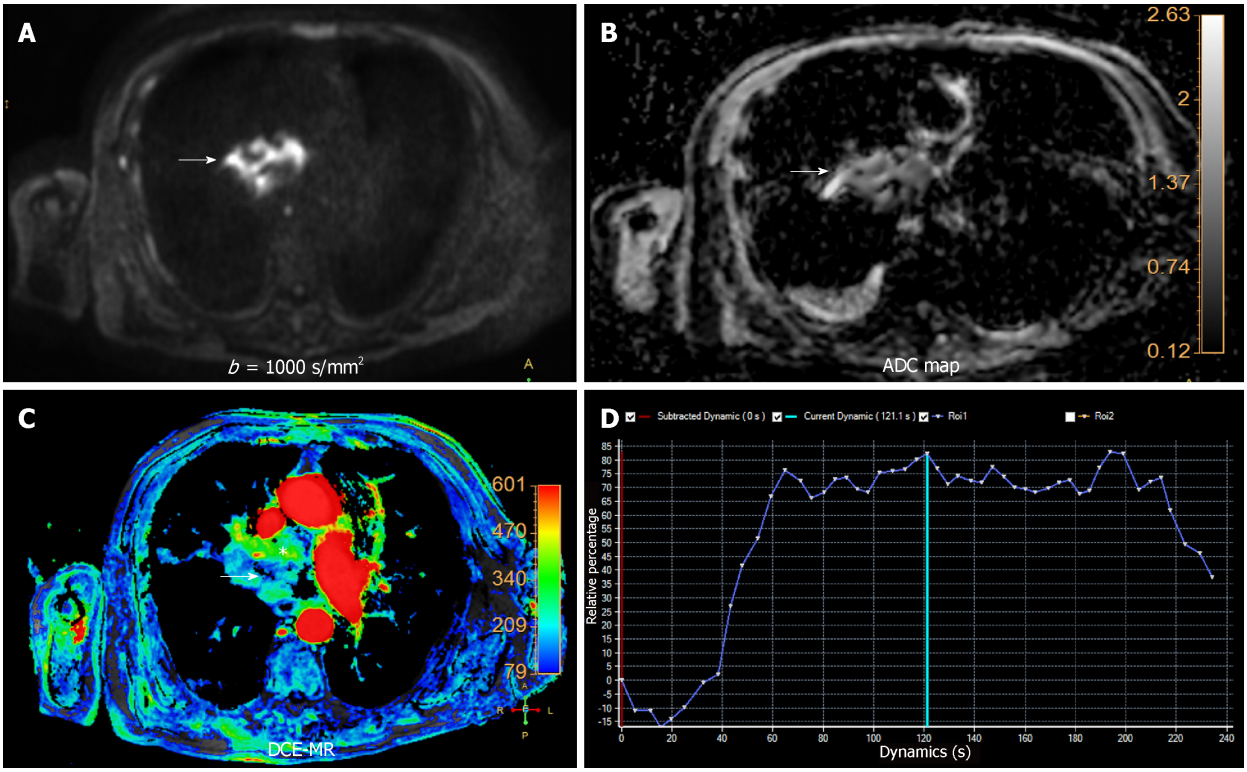

Figure 7 Multiparametric functional chest magnetic resonance of central lung cancer. A 78 year-old male with a central hilar mass in keeping with epidermoid type lung carcinoma. A and B: High *b* value (*b* = 1000 s/mm^2) and apparent diffusion coefficient (ADC) map (B) revealing a heterogeneous and restrictive behavior of the lesion, related to hypercellularity and aggressiveness (white arrows on A and B). The mean ADC was 0.97 × 10^{-3} mm^2/s, confirming a malignant origin; C: Dynamic contrast-enhanced magnetic resonance showing a significant uptake of gadolinium based contrast agent on area under the curve parametric map (white asterisk), with central necrosis (White arrow on C); D: Time intensity curve (TIC) plot revealing steep slope of enhancement with posterior plateau (type B TIC) also favoring a malignant etiology. DCE-MR: Dynamic contrast-enhanced magnetic resonance; ADC: Apparent diffusion coefficient; TIC: Time intensity curve.

therapeutic agents (vascular disrupting agents and immunotherapy). Because of the different mechanism of action in cancerous cells compared to conventional drugs, the radiologist must be conscious of the paradigmatic behavior of the lesions during treatment surveillance. Lung tumors with high ADC value are predictive of good response to vascular disrupting agents, and during the follow-up, a decrease of ADC is a sign of treatment effectiveness[8].

As well as in staging, the treatment response of esophageal cancer is made usually by ^{18}FDG-PET/CT. A decrease of more than 50% of the SUV_{max}/SUV_{mean} in the post-treatment follow-up compared to pre-treatment examination is in keeping with a good response. This method has low sensitivity and specificity (67%-70%), mainly due to chemotherapy and radiotherapy induced esophagitis. Also, the identification of a good response behavior precludes the detection of local recurrence, being present only in 42% of PET-based clinical responders[69]. On MRI, a difference in post-treatment ADC compared to pre-treatment value has been correlated with histopathological regression grade. This difference early on the treatment onset has a 100% predictive value on responders[76-78]. Therefore, the assessment of treatment effect with functional MR has a great potential utility in the differentiation of early response, with a possible impact in the prognosis of these patients (Figure 9).

CONCLUSION

Functional imaging of the mediastinum enhances an accurate assessment of mediastinal masses. It allows to distinguish with accuracy benign from malignant lesions. DWI and DCE-MRI are functional techniques which can be used in clinical protocols, providing an alternative to ^{18}FDG-PET/CT in the evaluation of mediastinal lesions. It allows a complete characterization of them in a one-stop-shop procedure, while avoiding the use of ionizing radiation. Functional techniques have a great potential impact in the staging of lung and esophageal cancers, increasing its precision, and in the therapy monitoring of mediastinal neoplasms. Quantitative functional MR-derived parameters provide unique information, which makes them authentic biomarkers with potential prognostic implications.

Table 5 Treatment monitoring and recurrence behavior

	Good response	Poor response
T2WI	No tumor ↑ SI in bone marrow	Residual/↑soft tissue mass ↑ extent bone marrow invasion
DWI	↑ ADC	↓ ADC
DCE-MRI	↓ slope/absent enhancement	Persistent / ↑ enhancement
MRS	↑ Choline peak	↓ Choline peak

T2WI: T2 weighted imaging; SI: Signal intensity; DWI: Diffusion weighted imaging; ADC: Apparent diffusion coefficient; DCE-MRI: Dynamic contrast enhanced magnetic resonance imaging; MRS: Magnetic resonance spectroscopy. Modified from Vilanova *et al*[18].

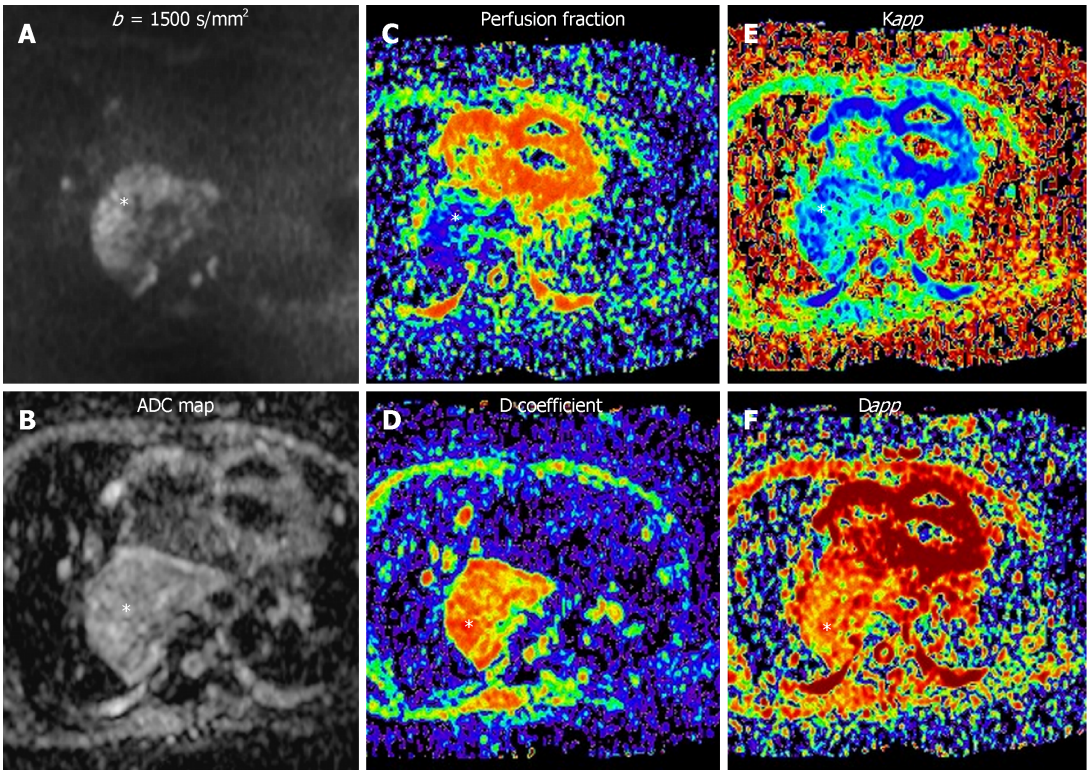

Figure 8 Different diffusion weighted imaging approaches to an aggressive middle mediastinal mass. A 56 year-old woman with esophageal leiomyosarcoma stage IV. A-F: Restrictive behavior of the mass could be seen [Apparent diffusion coefficient (ADC): 0.951 × 10^{-3} m^2/s; malignant origin]. Derived biomarkers of three different ways of quantification of diffusion-weighted imaging (white asterisk) of the mass are shown: A-B: Mono-exponential approach (A: High *b* value; B: ADC map); C-D: bi-exponential scheme (Intravoxel incoherent motion; C: Perfusion fraction map; D: Diffusion coefficient map); E-F: Diffusion kurtosis imaging (E: Apparent diffusional kurtosis map; F: Apparent diffusion map). ADC: Apparent diffusion coefficient.

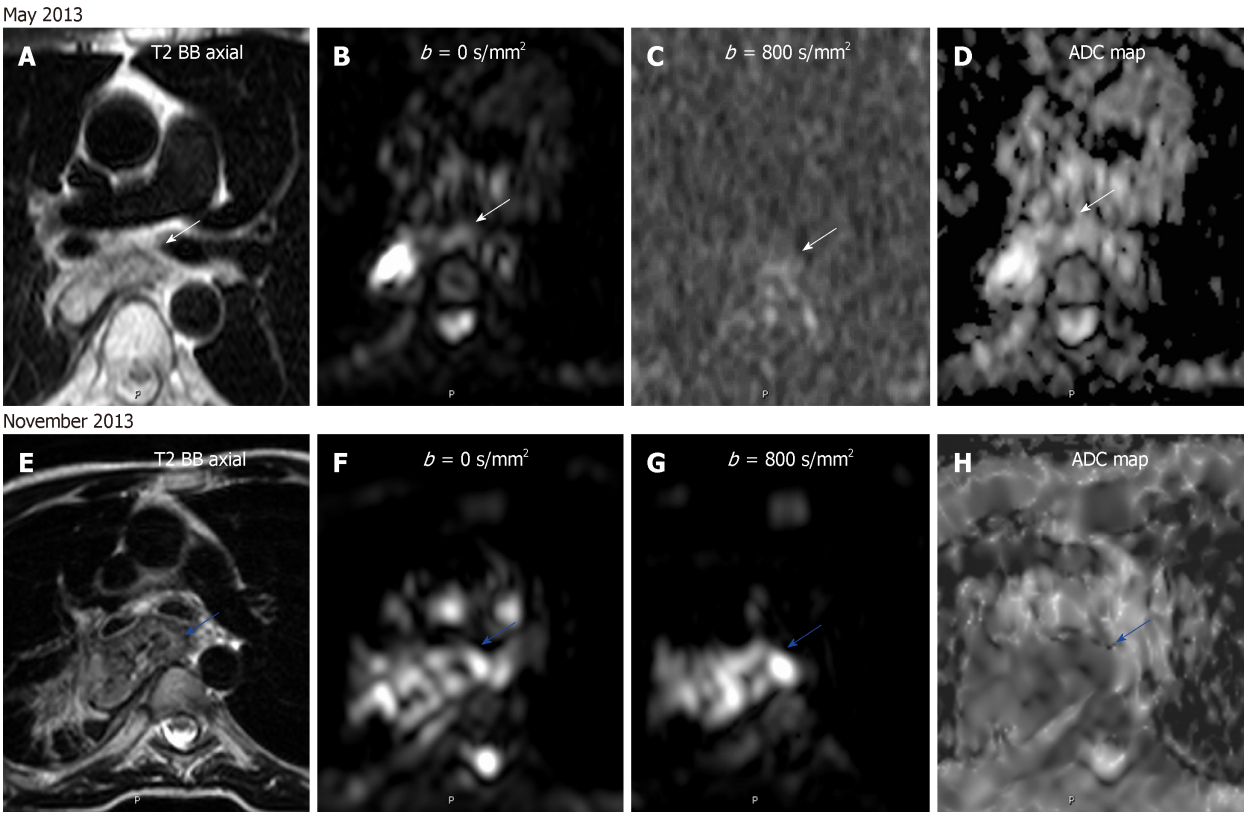

Figure 9 Treatment monitoring of an esophageal carcinoma by diffusion-weighted imaging. A 47 year-old male with esophageal carcinoma treated with esophagectomy and gastroplasty. A-D: Post-surgery surveillance magnetic resonance (MR) shows a normal appearing anastomosis on turbo spin echo (TSE) T2-weighted sequence and with no restriction on diffusion-weighted imaging and apparent diffusion coefficient (ADC) map (B-D; white arrows); D-G: Follow-up MR examination done 6 mo later revealing anastomotic thickening on TSE T2-weighted image and with restrictive behavior on diffusion-weighted whole-body imaging and ADC map (F-H), in keeping with relapse (blue arrows). ADC: Apparent diffusion coefficient.

REFERENCES

1 **Ackman JB**. MR Imaging of Mediastinal Masses. *Magn Reson Imaging Clin N Am* 2015; **23**: 141-164 [PMID: 25952512 DOI: 10.1016/j.mric.2015.01.002]
2 **Carter BW**, Benveniste MF, Truong MT, Marom EM. State of the Art: MR Imaging of Thymoma. *Magn Reson Imaging Clin N Am* 2015; **23**: 165-177 [PMID: 25952513 DOI: 10.1016/j.mric.2015.01.005]
3 **Carter BW**, Betancourt SL, Benveniste MF. MR Imaging of Mediastinal Masses. *Top Magn Reson Imaging* 2017; **26**: 153-165 [PMID: 28777164 DOI: 10.1097/RMR.0000000000000134]
4 **Razek AA**, Elmorsy A, Elshafey M, Elhadedy T, Hamza O. Assessment of mediastinal tumors with diffusion-weighted single-shot echo-planar MRI. *J Magn Reson Imaging* 2009; **30**: 535-540 [PMID: 19630080 DOI: 10.1002/jmri.21871]
5 **Yabuuchi H**, Matsuo Y, Abe K, Baba S, Sunami S, Kamitani T, Yonezawa M, Yamasaki Y, Kawanami S, Nagao M, Okamoto T, Nakamura K, Yamamoto H, Sasaki M, Honda H. Anterior mediastinal solid tumours in adults: Characterisation using dynamic contrast-enhanced MRI, diffusion-weighted MRI, and FDG-PET/CT. *Clin Radiol* 2015; **70**: 1289-1298 [PMID: 26272529 DOI: 10.1016/j.crad.2015.07.004]
6 **Broncano J**, Luna A, Sánchez-González J, Alvarez-Kindelan A, Bhalla S. Functional MR Imaging in Chest Malignancies. *Magn Reson Imaging Clin N Am* 2016; **24**: 135-155 [PMID: 26613879 DOI: 10.1016/j.mric.2015.08.004]
7 **Ciliberto M**, Kishida Y, Seki S, Yoshikawa T, Ohno Y. Update of MR Imaging for Evaluation of Lung Cancer. *Radiol Clin North Am* 2018; **56**: 437-469 [PMID: 29622078 DOI: 10.1016/j.rcl.2018.01.005]
8 **Bains LJ**, Zweifel M, Thoeny HC. Therapy response with diffusion MRI: An update. *Cancer Imaging* 2012; **12**: 395-402 [PMID: 23022595 DOI: 10.1102/1470-7330.2012.9047]
9 **Le Bihan D**. Apparent diffusion coefficient and beyond: What diffusion MR imaging can tell us about tissue structure. *Radiology* 2013; **268**: 318-322 [PMID: 23882093 DOI: 10.1148/radiol.13130420]
10 **Le Bihan D**, Breton E, Lallemand D, Aubin ML, Vignaud J, Laval-Jeantet M. Separation of diffusion and perfusion in intravoxel incoherent motion MR imaging. *Radiology* 1988; **168**: 497-505 [PMID: 3393671 DOI: 10.1148/radiology.168.2.3393671]
11 **Filippi M**, Agosta F. Diffusion tensor imaging and functional MRI. *Handb Clin Neurol* 2016; **136**: 1065-1087 [PMID: 27430459 DOI: 10.1016/B978-0-444-53486-6.00056-9]
12 **Huston JM**, Field AS. Clinical applications of diffusion tensor imaging. *Magn Reson Imaging Clin N Am* 2013; **21**: 279-298 [PMID: 23642554 DOI: 10.1016/j.mric.2012.12.003]
13 **Barrett T**, Brechbiel M, Bernardo M, Choyke PL. MRI of tumor angiogenesis. *J Magn Reson Imaging* 2007; **26**: 235-249 [PMID: 17623889 DOI: 10.1002/jmri.20991]
14 **Buonaccorsi GA**, Roberts C, Cheung S, Watson Y, O'Connor JP, Davies K, Jackson A, Jayson GC, Parker GJ. Comparison of the performance of tracer kinetic model-driven registration for dynamic contrast enhanced MRI using different models of contrast enhancement. *Acad Radiol* 2006; **13**: 1112-1123 [PMID:

16935723 DOI: 10.1016/j.acra.2006.05.016]
15 **Runge VM**, Clanton JA, Herzer WA, Gibbs SJ, Price AC, Partain CL, James AE. Intravascular contrast agents suitable for magnetic resonance imaging. *Radiology* 1984; **153**: 171-176 [PMID: 6433402 DOI: 10.1148/radiology.153.1.6433402]
16 **Rijpkema M**, Kaanders JH, Joosten FB, van der Kogel AJ, Heerschap A. Method for quantitative mapping of dynamic MRI contrast agent uptake in human tumors. *J Magn Reson Imaging* 2001; **14**: 457-463 [PMID: 11599071 DOI: 10.1002/jmri.1207]
17 **Luna A**, Pahwa S, Bonini C, Alcalá-Mata L, Wright KL, Gulani V. Multiparametric MR Imaging in Abdominal Malignancies. *Magn Reson Imaging Clin N Am* 2016; **24**: 157-186 [PMID: 26613880 DOI: 10.1016/j.mric.2015.08.005]
18 **Vilanova JC**, Baleato-Gonzalez S, Romero MJ, Carrascoso-Arranz J, Luna A. Assessment of Musculoskeletal Malignancies with Functional MR Imaging. *Magn Reson Imaging Clin N Am* 2016; **24**: 239-259 [PMID: 26613884 DOI: 10.1016/j.mric.2015.08.006]
19 **Vaupel P**, Mayer A. Hypoxia in cancer: Significance and impact on clinical outcome. *Cancer Metastasis Rev* 2007; **26**: 225-239 [PMID: 17440684 DOI: 10.1007/s10555-007-9055-1]
20 **Carter BW**, Tomiyama N, Bhora FY, Rosado de Christenson ML, Nakajima J, Boiselle PM, Detterbeck FC, Marom EM. A modern definition of mediastinal compartments. *J Thorac Oncol* 2014; **9**: S97-101 [PMID: 25396318 DOI: 10.1097/JTO.0000000000000292]
21 **Nishino M**, Ashiku SK, Kocher ON, Thurer RL, Boiselle PM, Hatabu H. The thymus: A comprehensive review. *Radiographics* 2006; **26**: 335-348 [PMID: 16549602 DOI: 10.1148/rg.262045213]
22 **Priola AM**, Priola SM, Ciccone G, Evangelista A, Cataldi A, Gned D, Pazè F, Ducco L, Moretti F, Brundu M, Veltri A. Differentiation of rebound and lymphoid thymic hyperplasia from anterior mediastinal tumors with dual-echo chemical-shift MR imaging in adulthood: Reliability of the chemical-shift ratio and signal intensity index. *Radiology* 2015; **274**: 238-249 [PMID: 25105246 DOI: 10.1148/radiol.14132665]
23 **Inaoka T**, Takahashi K, Mineta M, Yamada T, Shuke N, Okizaki A, Nagasawa K, Sugimori H, Aburano T. Thymic hyperplasia and thymus gland tumors: Differentiation with chemical shift MR imaging. *Radiology* 2007; **243**: 869-876 [PMID: 17463136 DOI: 10.1148/radiol.2433060797]
24 **Ackman JB**, Mino-Kenudson M, Morse CR. Nonsuppressing normal thymus on chemical shift magnetic resonance imaging in a young woman. *J Thorac Imaging* 2012; **27**: W196-W198 [PMID: 22487991 DOI: 10.1097/RTI.0b013e318249936a]
25 **Ackman JB**, Kovacina B, Carter BW, Wu CC, Sharma A, Shepard JA, Halpern EF. Sex difference in normal thymic appearance in adults 20-30 years of age. *Radiology* 2013; **268**: 245-253 [PMID: 23440318 DOI: 10.1148/radiol.13121104]
26 **Falkson CB**, Bezjak A, Darling G, Gregg R, Malthaner R, Maziak DE, Yu E, Smith CA, McNair S, Ung YC, Evans WK; Lung Cancer Disease Site Group of Cancer Care Ontario's Program in Evidence-Based Care. The management of thymoma: A systematic review and practice guideline. *J Thorac Oncol* 2009; **4**: 911-919 [PMID: 19557895 DOI: 10.1097/JTO.0b013e3181a4b8e0]
27 **Carter BW**, Benveniste MF, Madan R, Godoy MC, de Groot PM, Truong MT, Rosado-de-Christenson ML, Marom EM. ITMIG Classification of Mediastinal Compartments and Multidisciplinary Approach to Mediastinal Masses. *Radiographics* 2017; **37**: 413-436 [PMID: 28129068 DOI: 10.1148/rg.2017160095]
28 **Engels EA**. Epidemiology of thymoma and associated malignancies. *J Thorac Oncol* 2010; **5**: S260-S265 [PMID: 20859116 DOI: 10.1097/JTO.0b013e3181f1f62d]
29 **Levy Y**, Afek A, Sherer Y, Bar-Dayan Y, Shibi R, Kopolovic J, Shoenfeld Y. Malignant thymoma associated with autoimmune diseases: A retrospective study and review of the literature. *Semin Arthritis Rheum* 1998; **28**: 73-79 [PMID: 9806367 DOI: 10.1016/S0049-0172(98)80039-5]
30 **Sakai S**, Murayama S, Soeda H, Matsuo Y, Ono M, Masuda K. Differential diagnosis between thymoma and non-thymoma by dynamic MR imaging. *Acta Radiol* 2002; **43**: 262-268 [PMID: 12100322 DOI: 10.1080/j.1600-0455.2002.430306.x]
31 **Yao JC**, Hassan M, Phan A, Dagohoy C, Leary C, Mares JE, Abdalla EK, Fleming JB, Vauthey JN, Rashid A, Evans DB. One hundred years after "carcinoid": Epidemiology of and prognostic factors for neuroendocrine tumors in 35,825 cases in the United States. *J Clin Oncol* 2008; **26**: 3063-3072 [PMID: 18565894 DOI: 10.1200/JCO.2007.15.4377]
32 **Gaur P**, Leary C, Yao JC. Thymic neuroendocrine tumors: A SEER database analysis of 160 patients. *Ann Surg* 2010; **251**: 1117-1121 [PMID: 20485130 DOI: 10.1097/SLA.0b013e3181dd4ec4]
33 **Gibril F**, Chen YJ, Schrump DS, Vortmeyer A, Zhuang Z, Lubensky IA, Reynolds JC, Louie A, Entsuah LK, Huang K, Asgharian B, Jensen RT. Prospective study of thymic carcinoids in patients with multiple endocrine neoplasia type 1. *J Clin Endocrinol Metab* 2003; **88**: 1066-1081 [PMID: 12629087 DOI: 10.1210/jc.2002-021314]
34 **Nasseri F**, Eftekhari F. Clinical and radiologic review of the normal and abnormal thymus: Pearls and pitfalls. *Radiographics* 2010; **30**: 413-428 [PMID: 20228326 DOI: 10.1148/rg.302095131]
35 **Nishino M**, Ashiku SK, Kocher ON, Thurer RL, Boiselle PM, Hatabu H. The Thymus: A Comprehensive Review-Erratum. *Radiographics* 2017; **37**: 1004 [PMID: 28493794 DOI: 10.1148/rg.2017174002]
36 **Ried M**, Marx A, Götz A, Hamer O, Schalke B, Hofmann HS. State of the art: Diagnostic tools and innovative therapies for treatment of advanced thymoma and thymic carcinoma. *Eur J Cardiothorac Surg* 2016; **49**: 1545-1552 [PMID: 26670806 DOI: 10.1093/ejcts/ezv426]
37 **Duwe BV**, Sterman DH, Musani AI. Tumors of the mediastinum. *Chest* 2005; **128**: 2893-2909 [PMID: 16236967 DOI: 10.1378/chest.128.4.2893]
38 **Jemal A**, Siegel R, Ward E, Murray T, Xu J, Thun MJ. Cancer statistics, 2007. *CA Cancer J Clin* 2007; **57**: 43-66 [PMID: 17237035 DOI: 10.3322/canjclin.57.1.43]
39 **Siegel R**, Ward E, Brawley O, Jemal A. Cancer statistics, 2011: The impact of eliminating socioeconomic and racial disparities on premature cancer deaths. *CA Cancer J Clin* 2011; **61**: 212-236 [PMID: 21685461 DOI: 10.3322/caac.20121]
40 **Barrington SF**, Mikhaeel NG, Kostakoglu L, Meignan M, Hutchings M, Müeller SP, Schwartz LH, Zucca E, Fisher RI, Trotman J, Hoekstra OS, Hicks RJ, O'Doherty MJ, Hustinx R, Biggi A, Cheson BD. Role of imaging in the staging and response assessment of lymphoma: Consensus of the International Conference on Malignant Lymphomas Imaging Working Group. *J Clin Oncol* 2014; **32**: 3048-3058 [PMID: 25113771 DOI: 10.1200/JCO.2013.53.5229]
41 **Kulkarni NM**, Pinho DF, Narayanan S, Kambadakone AR, Abramson JS, Sahani DV. Imaging for Oncologic Response Assessment in Lymphoma. *AJR Am J Roentgenol* 2017; **208**: 18-31 [PMID: 27786547 DOI: 10.2214/AJR.16.16180]
42 **Younes A**, Hilden P, Coiffier B, Hagenbeek A, Salles G, Wilson W, Seymour JF, Kelly K, Gribben J,

Pfreunschuh M, Morschhauser F, Schoder H, Zelenetz AD, Rademaker J, Advani R, Valente N, Fortpied C, Witzig TE, Sehn LH, Engert A, Fisher RI, Zinzani PL, Federico M, Hutchings M, Bollard C, Trneny M, Elsayed YA, Tobinai K, Abramson JS, Fowler N, Goy A, Smith M, Ansell S, Kuruvilla J, Dreyling M, Thieblemont C, Little RF, Aurer I, Van Oers MHJ, Takeshita K, Gopal A, Rule S, de Vos S, Kloos I, Kaminski MS, Meignan M, Schwartz LH, Leonard JP, Schuster SJ, Seshan VE. International Working Group consensus response evaluation criteria in lymphoma (RECIL 2017). *Ann Oncol* 2017; **28**: 1436-1447 [PMID: 28379322 DOI: 10.1093/annonc/mdx097]

43 **Koşucu P**, Tekinbaş C, Erol M, Sari A, Kavgaci H, Oztuna F, Ersöz S. Mediastinal lymph nodes: Assessment with diffusion-weighted MR imaging. *J Magn Reson Imaging* 2009; **30**: 292-297 [PMID: 19629990 DOI: 10.1002/jmri.21850]

44 **Mosavi F**, Wassberg C, Selling J, Molin D, Ahlström H. Whole-body diffusion-weighted MRI and (18)F-FDG PET/CT can discriminate between different lymphoma subtypes. *Clin Radiol* 2015; **70**: 1229-1236 [PMID: 26208992 DOI: 10.1016/j.crad.2015.06.087]

45 **Rosado-de-Christenson ML**, Templeton PA, Moran CA. From the archives of the AFIP. Mediastinal germ cell tumors: Radiologic and pathologic correlation. *Radiographics* 1992; **12**: 1013-1030 [PMID: 1326777 DOI: 10.1148/radiographics.12.5.1326777]

46 **Molinari F**, Bankier AA, Eisenberg RL. Fat-containing lesions in adult thoracic imaging. *AJR Am J Roentgenol* 2011; **197**: W795-W813 [PMID: 22021525 DOI: 10.2214/AJR.11.6932]

47 **Carter BW**, Okumura M, Detterbeck FC, Marom EM. Approaching the patient with an anterior mediastinal mass: A guide for radiologists. *J Thorac Oncol* 2014; **9**: S110-S118 [PMID: 25396307 DOI: 10.1097/JTO.0000000000000295]

48 **Strollo DC**, Rosado-de-Christenson ML. Primary mediastinal malignant germ cell neoplasms: Imaging features. *Chest Surg Clin N Am* 2002; **12**: 645-658 [PMID: 12471868 DOI: 10.1016/S1052-3359(02)00026-1]

49 **Lemarié E**, Assouline PS, Diot P, Regnard JF, Levasseur P, Droz JP, Ruffié P. Primary mediastinal germ cell tumors. Results of a French retrospective study. *Chest* 1992; **102**: 1477-1483 [PMID: 1330448 DOI: 10.1378/chest.102.5.1477]

50 **Economou JS**, Trump DL, Holmes EC, Eggleston JE. Management of primary germ cell tumors of the mediastinum. *J Thorac Cardiovasc Surg* 1982; **83**: 643-649 [PMID: 7200560]

51 **Kesler KA**, Rieger KM, Ganjoo KN, Sharma M, Fineberg NS, Einhorn LH, Brown JW. Primary mediastinal nonseminomatous germ cell tumors: The influence of postchemotherapy pathology on long-term survival after surgery. *J Thorac Cardiovasc Surg* 1999; **118**: 692-700 [PMID: 10504636 DOI: 10.1016/S0022-5223(99)70015-2]

52 **Wright CD**, Kesler KA, Nichols CR, Mahomed Y, Einhorn LH, Miller ME, Brown JW. Primary mediastinal nonseminomatous germ cell tumors. Results of a multimodality approach. *J Thorac Cardiovasc Surg* 1990; **99**: 210-217 [PMID: 2153877 DOI: 10.1016/0022-4804(90)90209-K]

53 **Lee KS**, Im JG, Han CH, Han MC, Kim CW, Kim WS. Malignant primary germ cell tumors of the mediastinum: CT features. *AJR Am J Roentgenol* 1989; **153**: 947-951 [PMID: 2552783 DOI: 10.2214/ajr.153.5.947]

54 **Shi HF**, Feng Q, Qiang JW, Li RK, Wang L, Yu JP. Utility of diffusion-weighted imaging in differentiating malignant from benign thyroid nodules with magnetic resonance imaging and pathologic correlation. *J Comput Assist Tomogr* 2013; **37**: 505-510 [PMID: 23863524 DOI: 10.1097/RCT.0b013e31828d28f0]

55 **Schob S**, Voigt P, Bure L, Meyer HJ, Wickenhauser C, Behrmann C, Höhn A, Kachel P, Dralle H, Hoffmann KT, Surov A. Diffusion-Weighted Imaging Using a Readout-Segmented, Multishot EPI Sequence at 3 T Distinguishes between Morphologically Differentiated and Undifferentiated Subtypes of Thyroid Carcinoma-A Preliminary Study. *Transl Oncol* 2016; **9**: 403-410 [PMID: 27661405 DOI: 10.1016/j.tranon.2016.09.001]

56 **Juanpere S**, Cañete N, Ortuño P, Martínez S, Sanchez G, Bernado L. A diagnostic approach to the mediastinal masses. *Insights Imaging* 2013; **4**: 29-52 [PMID: 23225215 DOI: 10.1007/s13244-012-0201-0]

57 **Kukar M**, Platz TA, Schaffner TJ, Elmarzouky R, Groman A, Kumar S, Abdelhalim A, Cance WG. The use of modified four-dimensional computed tomography in patients with primary hyperparathyroidism: An argument for the abandonment of routine sestamibi single-positron emission computed tomography (SPECT). *Ann Surg Oncol* 2015; **22**: 139-145 [PMID: 25074663 DOI: 10.1245/s10434-014-3940-y]

58 **Rodgers SE**, Hunter GJ, Hamberg LM, Schellingerhout D, Doherty DB, Ayers GD, Shapiro SE, Edeiken BS, Truong MT, Evans DB, Lee JE, Perrier ND. Improved preoperative planning for directed parathyroidectomy with 4-dimensional computed tomography. *Surgery* 2006; **140**: 932-40; discussion 940-1 [PMID: 17188140 DOI: 10.1016/j.surg.2006.07.028]

59 **Matoba M**, Tonami H, Kondou T, Yokota H, Higashi K, Toga H, Sakuma T. Lung carcinoma: Diffusion-weighted mr imaging--preliminary evaluation with apparent diffusion coefficient. *Radiology* 2007; **243**: 570-577 [PMID: 17400757 DOI: 10.1148/radiol.2432060131]

60 **Koyama H**, Ohno Y, Seki S, Nishio M, Yoshikawa T, Matsumoto S, Maniwa Y, Itoh T, Nishimura Y, Sugimura K. Value of diffusion-weighted MR imaging using various parameters for assessment and characterization of solitary pulmonary nodules. *Eur J Radiol* 2015; **84**: 509-515 [PMID: 25554007 DOI: 10.1016/j.ejrad.2014.11.024]

61 **Gümüştaş S**, Inan N, Akansel G, Ciftçi E, Demirci A, Ozkara SK. Differentiation of malignant and benign lung lesions with diffusion-weighted MR imaging. *Radiol Oncol* 2012; **46**: 106-113 [PMID: 23077446 DOI: 10.2478/v10019-012-0021-3]

62 **Liu H**, Liu Y, Yu T, Ye N. Usefulness of diffusion-weighted MR imaging in the evaluation of pulmonary lesions. *Eur Radiol* 2010; **20**: 807-815 [PMID: 19862533 DOI: 10.1007/s00330-009-1629-6]

63 **Coolen J**, Vansteenkiste J, De Keyzer F, Decaluwé H, De Wever W, Deroose C, Dooms C, Verbeken E, De Leyn P, Vandecaveye V, Van Raemdonck D, Nackaerts K, Dymarkowski S, Verschakelen J. Characterisation of solitary pulmonary lesions combining visual perfusion and quantitative diffusion MR imaging. *Eur Radiol* 2014; **24**: 531-541 [PMID: 24173597 DOI: 10.1007/s00330-013-3053-1]

64 **Schaefer JF**, Vollmar J, Schick F, Vonthein R, Seemann MD, Aebert H, Dierkesmann R, Friedel G, Claussen CD. Solitary pulmonary nodules: Dynamic contrast-enhanced MR imaging--perfusion differences in malignant and benign lesions. *Radiology* 2004; **232**: 544-553 [PMID: 15215548 DOI: 10.1148/radiol.2322030515]

65 **Donmez FY**, Yekeler E, Saeidi V, Tunaci A, Tunaci M, Acunas G. Dynamic contrast enhancement patterns of solitary pulmonary nodules on 3D gradient-recalled echo MRI. *AJR Am J Roentgenol* 2007;

189: 1380-1386 [PMID: 18029874 DOI: 10.2214/AJR.07.2429]
66 **Kono R**, Fujimoto K, Terasaki H, Müller NL, Kato S, Sadohara J, Hayabuchi N, Takamori S. Dynamic MRI of solitary pulmonary nodules: Comparison of enhancement patterns of malignant and benign small peripheral lung lesions. *AJR Am J Roentgenol* 2007; **188**: 26-36 [PMID: 17179342 DOI: 10.2214/AJR.05.1446]
67 **Chhabra A**, Thakkar RS, Andreisek G, Chalian M, Belzberg AJ, Blakeley J, Hoke A, Thawait GK, Eng J, Carrino JA. Anatomic MR imaging and functional diffusion tensor imaging of peripheral nerve tumors and tumorlike conditions. *AJNR Am J Neuroradiol* 2013; **34**: 802-807 [PMID: 23124644 DOI: 10.3174/ajnr.A3316]
68 **Nomori H**, Mori T, Ikeda K, Kawanaka K, Shiraishi S, Katahira K, Yamashita Y. Diffusion-weighted magnetic resonance imaging can be used in place of positron emission tomography for N staging of non-small cell lung cancer with fewer false-positive results. *J Thorac Cardiovasc Surg* 2008; **135**: 816-822 [PMID: 18374761 DOI: 10.1016/j.jtcvs.2007.10.035]
69 **van Rossum PS**, van Lier AL, Lips IM, Meijer GJ, Reerink O, van Vulpen M, Lam MG, van Hillegersberg R, Ruurda JP. Imaging of oesophageal cancer with FDG-PET/CT and MRI. *Clin Radiol* 2015; **70**: 81-95 [PMID: 25172205 DOI: 10.1016/j.crad.2014.07.017]
70 **Sakurada A**, Takahara T, Kwee TC, Yamashita T, Nasu S, Horie T, Van Cauteren M, Imai Y. Diagnostic performance of diffusion-weighted magnetic resonance imaging in esophageal cancer. *Eur Radiol* 2009; **19**: 1461-1469 [PMID: 19172278 DOI: 10.1007/s00330-008-1291-4]
71 **Takenaka D**, Ohno Y, Matsumoto K, Aoyama N, Onishi Y, Koyama H, Nogami M, Yoshikawa T, Matsumoto S, Sugimura K. Detection of bone metastases in non-small cell lung cancer patients: Comparison of whole-body diffusion-weighted imaging (DWI), whole-body MR imaging without and with DWI, whole-body FDG-PET/CT, and bone scintigraphy. *J Magn Reson Imaging* 2009; **30**: 298-308 [PMID: 19629984 DOI: 10.1002/jmri.21858]
72 **Ohno Y**, Koyama H, Onishi Y, Takenaka D, Nogami M, Yoshikawa T, Matsumoto S, Kotani Y, Sugimura K. Non-small cell lung cancer: Whole-body MR examination for M-stage assessment--utility for whole-body diffusion-weighted imaging compared with integrated FDG PET/CT. *Radiology* 2008; **248**: 643-654 [PMID: 18539889 DOI: 10.1148/radiol.2482072039]
73 **Yi CA**, Shin KM, Lee KS, Kim BT, Kim H, Kwon OJ, Choi JY, Chung MJ. Non-small cell lung cancer staging: Efficacy comparison of integrated PET/CT versus 3.0-T whole-body MR imaging. *Radiology* 2008; **248**: 632-642 [PMID: 18552311 DOI: 10.1148/radiol.2482071822]
74 **Yabuuchi H**, Hatakenaka M, Takayama K, Matsuo Y, Sunami S, Kamitani T, Jinnouchi M, Sakai S, Nakanishi Y, Honda H. Non-small cell lung cancer: Detection of early response to chemotherapy by using contrast-enhanced dynamic and diffusion-weighted MR imaging. *Radiology* 2011; **261**: 598-604 [PMID: 21852569 DOI: 10.1148/radiol.11101503]
75 **Ohno Y**, Koyama H, Yoshikawa T, Matsumoto K, Aoyama N, Onishi Y, Sugimura K. Diffusion-weighted MRI versus 18F-FDG PET/CT: Performance as predictors of tumor treatment response and patient survival in patients with non-small cell lung cancer receiving chemoradiotherapy. *AJR Am J Roentgenol* 2012; **198**: 75-82 [PMID: 22194481 DOI: 10.2214/AJR.11.6525]
76 **van Rossum PS**, van Lier AL, van Vulpen M, Reerink O, Lagendijk JJ, Lin SH, van Hillegersberg R, Ruurda JP, Meijer GJ, Lips IM. Diffusion-weighted magnetic resonance imaging for the prediction of pathologic response to neoadjuvant chemoradiotherapy in esophageal cancer. *Radiother Oncol* 2015; **115**: 163-170 [PMID: 26002307 DOI: 10.1016/j.radonc.2015.04.027]
77 **Wang L**, Liu L, Han C, Liu S, Tian H, Li Z, Ren X, Shi G, Wang Q, Wang G. The diffusion-weighted magnetic resonance imaging (DWI) predicts the early response of esophageal squamous cell carcinoma to concurrent chemoradiotherapy. *Radiother Oncol* 2016; **121**: 246-251 [PMID: 27838148 DOI: 10.1016/j.radonc.2016.10.021]
78 **Giganti F**, Salerno A, Ambrosi A, Chiari D, Orsenigo E, Esposito A, Albarello L, Mazza E, Staudacher C, Del Maschio A, De Cobelli F. Prognostic utility of diffusion-weighted MRI in oesophageal cancer: Is apparent diffusion coefficient a potential marker of tumour aggressiveness? *Radiol Med* 2016; **121**: 173-180 [PMID: 26392393 DOI: 10.1007/s11547-015-0585-2]

World Journal of Radiology

Submit a Manuscript: https://www.f6publishing.com

World J Radiol 2019 March 28; 11(3): 46-54

DOI: 10.4329/wjr.v11.i3.46

ISSN 1949-8470 (online)

MINIREVIEWS

Progress in image-guided radiotherapy for the treatment of non-small cell lung cancer

Xiao-Cang Ren, Yue-E Liu, Jing Li, Qiang Lin

ORCID number: Xiao-Cang Ren (0000-0001-5632-1434); Yue-E Liu (0000-0002-4222-2061); Jing Li (0000-0003-1724-3490); Qiang Lin (0000-0001-9599-4121).

Author contributions: Ren XC wrote the manuscript; Liu YE and Li J contributed to the writing of the manuscript; Lin Q designed the editorial and wrote the manuscript.

Conflict-of-interest statement: There is no conflict of interest associated with any of the senior author or other coauthors contributed their efforts in this manuscript.

Manuscript source: Invited manuscript

Received: October 29, 2018
Peer-review started: October 29, 2018
First decision: November 29, 2018
Revised: January 27, 2019
Accepted: February 27, 2019
Article in press: March 28, 2019

Xiao-Cang Ren, Yue-E Liu, Jing Li, Qiang Lin, Department of Oncology, North China Petroleum Bureau General Hospital, Hebei Medical University, Renqiu 062552, Hebei Province, China

Corresponding author: Qiang Lin, MD, PhD, Professor, Department of Oncology, North China Petroleum Bureau General Hospital, Hebei Medical University, 8 Huizhan Avenue, Renqiu 062552, Hebei Province, China. zyy_lq@petrochina.com.cn
Telephone: +86-317-2721951
Fax: +86-317-2722381

Abstract

Lung cancer is one of the most common malignant tumors. It has the highest incidence and mortality rate of all cancers worldwide. Late diagnosis of non-small cell lung cancer (NSCLC) is very common in clinical practice, and most patients miss the chance for radical surgery. Thus, radiotherapy plays an indispensable role in the treatment of NSCLC. Radiotherapy technology has evolved from the classic two-dimensional approach to three-dimensional conformal and intensity-modulated radiotherapy. However, how to ensure delivery of an accurate dose to the tumor while minimizing the irradiation of normal tissues remains a huge challenge for radiation oncologists, especially due to the positioning error between fractions and the autonomous movement of organs. In recent years, image-guided radiotherapy (IGRT) has greatly increased the accuracy of tumor irradiation while reducing the irradiation dose delivered to healthy tissues and organs. This paper presents a brief review of the definition of IGRT and the various technologies and applications of IGRT. IGRT can help ensure accurate dosing of the target area and reduce radiation damage to the surrounding normal tissue. IGRT may increase the local control rate of tumors and reduce the incidence of radio-therapeutic complications.

Key words: Non-small cell lung cancer; Radiotherapy; Image-guided radiotherapy; Intensity-modulated radiotherapy; Positioning error

Core tip: Lung cancer is one of the most common malignant tumors. Radiotherapy plays an indispensable role in the treatment of non-small cell lung cancer. How to ensure delivery of an accurate dose to the tumor while minimizing the irradiation of normal tissues remains a huge challenge. In this brief review, we summarize the methods of radiotherapy technology, especially for the image-guided radiotherapy (IGRT). We believe that IGRT can help ensure accurate dosing of the target area and reduce radiation

Published online: March 28, 2019

P-Reviewer: Bazeed MF, Engin G, Liang Y, Neninger E, Peitsidis P
S-Editor: Ji FF
L-Editor: A
E-Editor: Wu YXJ

damage to the surrounding normal tissue.

Citation: Ren XC, Liu YE, Li J, Lin Q. Progress in image-guided radiotherapy for the treatment of non-small cell lung cancer. *World J Radiology* 2019; 11(3): 46-54
URL: https://www.wjgnet.com/1949-8470/full/v11/i3/46.htm
DOI: https://dx.doi.org/10.4329/wjr.v11.i3.46

INTRODUCTION

Lung cancer is one of the most common malignant tumors, and it ranks first in both incidence and mortality worldwide. Non-small cell lung cancer (NSCLC) accounts for 80%-85% of all lung cancers[1]. Late diagnosis of NSCLC is very common in clinical practice, and most patients miss the chance for radical surgery. Thus, radiotherapy is one of major treatment modalities for NSCLC[1]. In recent years, continuous advancements in image-guided radiotherapy (IGRT) technology have enabled more accurate positioning and precise radiotherapy. IGRT can decrease errors during treatment, increase the local radiation dose, and reduce the dose of radiation delivered to the normal surrounding tissue to optimize the local tumor control rate and significantly improve patient quality of life[2,3]. This paper presents a brief review of the technical developments and application of IGRT in recent years.

STATUS OF RADIOTHERAPY

Lung cancer has increased globally in both incidence and mortality. It ranks first among malignant tumors in both incidence and mortality worldwide and is a threat to human health. NSCLC account for 80%-85% of all lung cancers, and early diagnosis is limited. Approximately 85% of patients are in advanced stages at the time of diagnosis. The efficacy of surgical treatment is not ideal, and the 5-year survival rate is only about 16%[4]. According to statistics radiotherapy was widely utilized as high as 55% in all new cancer cases[5]. In traditional two-dimensional radiotherapy, an oncologist must control the treatment based on his experience because the imaging diagnosis and positioning system operate on a two-dimensional plane. Irradiating a large area can easily destroy normal cells around the tumor but not the tumor itself. Therefore, the treatment efficacy is poor, with obvious side effects and many complications[6]. The ideal radiotherapy technique is to deliver a lethal dose to the target area according to the shape of the tumor without irradiating the normal tissue around the target area. In 1959, Dr. Takahashi from Japan first proposed and outlined the concept of conformal radiation therapy. The development and application of technologies such as computed tomography (CT), magnetic resonance imaging, three-dimensional treatment planning systems and multi-leaf collimators have made three-dimensional conformal radiotherapy possible and facilitated the transition from the 2-dimensional era to the 3-dimensional era. In recent years, many new technologies and new methods for improving the accuracy of treatment have been developed. Technologies such as three-dimensional conformal radiation therapy (3DCRT) and intensity-modulated radiation therapy (IMRT) have solved the problem of dose conformation in stationary target areas. However, the position and shape of the tumor and the positional relationship between the tumor and its surrounding organs can change over the course of treatment. The proactive treatment method uses a certain technique to detect the positioning error and/or movement of the target area and to improve the delivery of radiation to the tumor while correcting the error to better protect the surrounding normal tissues. Methods to ensure and control the quality of radiation therapy are still under active investigation.

DEFINITION OF IGRT

Compared to traditional radiotherapy, IGRT enhances the biological effects of radiotherapy and is considered an extension of 3DCRT and IMRT. It integrates respiratory movement over time during treatment and positioning error between fractions. It is the most advanced four-dimensional radiotherapy technology in the field of tumor treatment, featuring accurate positioning, plan design and control of

the accelerators. IGRT can correct the patient's positioning error, aid in planning subsequent radiotherapy, guide real-time beam irradiation, and collect images and/or other signals during treatment in order to ensure the accuracy of radiation delivery. The collected images and/or signals are used to guide and deliver the dose of radiation to the target area and ultimately improve the rate of local control rate and long-term survival in patients with advanced NSCLC[7-9]. IGRT technology can correct the error between the lesions and the markers and modify the changes in the radiation dose between the tumor and normal tissues. It can reasonably adjust the dose to protect normal tissue while reducing the safe marginal region and increasing dose delivery to the tumor area[10]. IGRT can be achieved using the following technologies: online correction, adaptive radiotherapy, breath-holding and respiratory gating control, four-dimensional radiotherapy and real-time tracking technology[11].

IMPLEMENTATION OF IGRT IN NSCLC RADIOTHERAPY

Online correction technology

During the course of fractional treatments, two-dimensional or three-dimensional images of the patient are acquired and compared to the planned image (preplaced markers) after positioning to determine the positioning error or the error of the radiation field, which are corrected immediately to obtain the appropriate position of the target area. The optimal radiation dose can then be delivered. In recent years, online correction has evolved from earlier film to current electro phoretic image display technology, which increases the degree of automation and shortens the additional treatment time. Moreover, the X-ray source for imaging has evolved from MV imaging to KV-MV combination imaging or KV imaging alone, and the technology for the calibration image has also evolved from two-dimensional to three-dimensional imaging such as spiral CT or cone beam CT (CBCT)[10,11].

Adaptive radiotherapy

Due to individual differences, the actual appropriate width of the marginal region around the target areas different for each patient. Therefore, it is necessary to set an individualized width of the marginal region according to the individual's positioning error and organ movement data and then to adjust the margins of the planned target volume (PTV) and the clinical target volume. The plan and mode of adaptive radiation therapy can be modified using a systematic feedback of measurements during treatment[12,13].

CBCT-guided adaptive radiotherapy: Conventional radiotherapy plans are designed based on CT images obtained before radiotherapy. However, changes in the patient's body mass index, tumor deformation, and movement of the surrounding organs can cause displacement of the target and consequent deformation[14]. CBCT-guided adaptive radiotherapy is a new extension of IGRT technology that allows for feedback of the target tumor volume and position changes during treatment to analyze the difference between the original plan and the treatment and to obtain real-time anatomical images in order to re-design the treatment plan. This technique can ensure appropriate dose delivery to the target area and reduce unnecessary irradiation of normal tissue, thus minimizing the side effects of radiotherapy[15,16]. A study by Zhao *et al*[17] described how to delineate the target area using the anatomical images collected by CBCT and how to form an outline of the new target area using deformation registration software. Under the guidance of CBCT, the treatment plan can be re-optimized. CBCT also allows for updated calculations of the actual dose accumulation in the target area and surrounding organs and an accurate final determination of the radiation dose for further treatments in order to reduce damage to normal tissues and increase dose delivery to the target area. Buckley *et al*[18] proposed CBCT-guided helical tomotherapy (HT) as a replacement for IMRT to achieve adaptive contour delineation, planning, and fractional dose accumulation. Currently, studies of CBCT-guided radiotherapy for NSCLC mainly focus on respiratory movement and shrinkage of the target area. Interference of respiratory movement can be improved by techniques such as respiratory gating, real-time tracking and 4D-CT, while the effect of target shrinkage can be effectively addressed by the timely modification of radiotherapy plans[19]. Adaptive radiotherapy technology based on CBCT image guidance could be comparable to adaptive HT with further optimization of the time required for adaptive radiotherapy planning. De *et al*[20] reported that HT and IGRT are effective and safe treatment modalities for anal cancer and are considered standard of care for these conditions in our department. A study by Elsayad *et al*[17] demonstrated 83% tumor regression and 13% progression in patients with small cell lung cancer (13 patients) or NSCLC (59 patients) undergoing

fractional CBCT-guided radiation. Moreover, the decrease in gross tumor volume was associated with the number of CBCT scans (r = 0.313, P = 0.046) and the time of chemotherapy administration (r = 0.385, P = 0.013). Weekly CBCT to monitor changes in the tumor offers the advantage of adaptive treatment for patients with lung cancer.

Breath-holding and respiratory gating technology

If the target area is affected by respiratory movement, breath-holding can temporarily eliminate such movement, allowing for a small marginal region. Before treatment, the patient should perform appropriate breathing exercises to increase the duration of breath-holding during treatment and to reduce the volume of lung radiation exposure[21,22]. Active respiratory gating technology and deep inspiration breath hold techniques are the two options available to minimize the influence of respiratory movement. Respiratory gating is a technique that collects images from different respiratory phases in NSCLC patients and reconstructs images by using four-dimensional computed tomography (4D-CT). It can be used to calculate and reconstruct doses at different respiratory phases to better eliminate movement artifacts, adjust the radiation plan, and monitor the effects of the patient's respiratory movement on the organ and target tumor area during treatment. Ultimately, this technique allows for control of the intensity of the radiation beam to the linear accelerator and matches the specific phase of the respiratory cycle of NSCLC patients with the controlled radiation beam[23-25]. Respiratory gating technology can reduce the influence of respiratory movement on radiotherapy. For instance, patients with stage I to II lung cancer who are affected by respiratory movements and patients with sub-phrenic tumors are better suited to respiratory gating technology with hypo-fractionated radiation therapy.

During radiotherapy, respiratory and organ movement in NSCLC patients causes movement of the tumor target area and displacement of the tumor's position in the lung, resulting in differences in anatomical position between the planned design and actual treatment. Moreover, changes in the volume and density of the lung tissue result in beam penumbra changes in the field and a lower dose of radiation delivery to the tumor target in lung tissue. Therefore, during IGLFRT, in addition to expansion of the radiation target area, assisted respiratory gating technology can help reduce the scope of treatment while increasing dose delivery to the tumor target area. This can effectively avert the possibility of mistargeted dose delivery and the consequent excessive exposure of normal tissue to radiation due to individual differences in respiratory movement[26].

Radiotherapy techniques accounting for time

Three-dimensional radiotherapy technology can be further enhanced by accounting for time using a technique that accounts for changes in anatomical structure during imaging positioning, planning, and therapeutic implementation. Three key factors must be taken into consideration: four-dimensional image localization (collecting the time sequence of four-dimensional images throughout all phases in one respiratory cycle), four-dimensional plan design (determination of time-marked field parameters from four-dimensional image data), and four-dimensional treatment implementation (monitoring of the patient's breathing using the same respiratory monitoring device used in the four-dimensional imaging system)[27,28].

Personalized delineation of the target range based on 4D-CT: During the course of routine spiral CT scanning, movement artifacts can cause up to 90% volumetric deviation in the 3D reconstruction of the target area. Therefore, it is very important to individualize the target range of movement in NSCLC patients[29]. The development of 4D-CT technology not only effectively eliminates movement artifacts to accurately and reliably reproduce the target area receiving radiotherapy but also can reflect the dynamic characteristics of radiotherapy in the target area with respect to respiratory movements and perform precise, individualized delineation of the target area[30]. 4D-CT takes advantage of three-dimensional reconstruction technology and integrates a time factor during image positioning, planning and treatment implementation stages. It also incorporates changes in anatomical structure over time, individualized target volume (ITV) changes and respiratory cycle. A study by Tan *et al*[31] has shown that 4D-CBCT is superior to 3D-CBCT in image guidance in small lung tumors because 4D-CBCT can reduce the uncertainty of the tumor location caused by internal respiratory movement, thereby increasing the accuracy of image guidance. Ehrbar *et al*[32] used 4D-CT to delineate ITV and design a radiotherapy plan for patients with lung cancer. Their results show that ITV ensured tumor coverage but that the lung tissue was exposed to higher doses of radiation. Significantly reduced ITV can improve tumor control while protecting normal tissues. In addition, Jurkovic *et al*[33] used the average intensity projection and maximum intensity projection techniques to

quickly and accurately delineate ITV. These techniques can significantly reduce the physical effort involved in target delineation. ITV delineation based on 4D-CT can increase the target dose and reduce the marginal region, thus reducing the radiation dose delivered to normal lung tissue.

Real-time tracking with stereotactic body radiotherapy

Because human respiratory movement is not strictly identical between two consecutive cycles, and treatment time is often longer than the image positioning time, especially when using hypofractional techniques (such as stereotactic radiotherapy), involuntary movements cannot be predicted. Real-time X-ray tracking treatment techniques have been developed to address this problem.

Image-guided hypofractionated stereotactic radiotherapy after accurate positioning in NSCLC patients can deliver large doses to the tumor target area, whereas the dose of radiation delivered to surrounding normal lung tissue is decreased[7,34]. The tumor control rate of conventional radiotherapy is low in some patients with early NSCLC who are not candidates for surgical treatment. IGRT treatment can reduce the uncertainty of the positioning error and the movement of the target area, thereby reducing the irradiation volume, which can allow for increased daily treatment doses, shortened treatment time, and improved local control[35]. For patients undergoing hypofractionated stereotactic radiotherapy, during the course of treatment, image guidance techniques are used to correct positioning errors and to monitor changes in tumor volume and location, thus ensuring coverage of the target area and reducing the dose absorbed by surrounding tissues[36,37]. A study by Ehrbar *et al*[32] showed that the control rate and overall survival of patients undergoing hypofractionated stereotactic treatment are superior to those of patients receiving conventional radiotherapy. Moreover, side effects were less common with hypofractionated radiotherapy. Verma *et al*[38] evaluated 92 patients from 12 institutions and found from their multi-institutional study that the toxicity of stereotactic body radiotherapy (SBRT) in patients with NSCLC tumors ≥ 5 cm was acceptable. Daily treatment are associated with a high toxicity rate. Vivek *et al*[39] reported that the 1- and 2-year actuarial local control rates in patients with NSCLC tumors ≥ 5 cm were 95.7% and 73.2%, respectively, and the 1-year and 2-year disease-free survival rates were 72.1% and 53.5%, respectively; the 1- and 2-year disease-specific survival rates were 95.5% and 78.6%, respectively. Their study indicates that SBRT is a safe and effective treatment when combined with IGRT technology (Figure 1 and Table 1).

CONCLUSION

In summary, image-guided hypofractionated radiotherapy has several advantages in the treatment of NSCLC. Functional imaging allows for the differentiation of normal tissue from tumor tissue. By ensuring radiotherapy accuracy and appropriate dosing, these technologies can lower the radiation dose delivered to normal surrounding tissue while improving the local tumor control rate of the tumor and reducing the chance of radiation complications. This results in improved the quality of life of patients after treatment. Treatment that is based on advanced image guidance technology and computer-assisted adaptive radiotherapy is likely to become the most common approach for NSCLC radiotherapy in the future.

Table 1 Summary of important data of advantage of image-guided radiotherapy in radiotherapy

Ref.	Published date	Authors	Highlights of detailed data
[21]	2003	Remouchamps *et al*	The use of mDIBH reduced the mean percentage of both lungs receiving more than 20 Gy from 20.4% to 15.2% ($P < 0.00007$)
[22]	2015	Muralidhar *et al*	The mean difference of right lung volume receiving more than 20 Gy of the dose was from 1% to -98 % (IGRT < 0.24556)
[26]	2003	Hof *et al*	In the craniocaudal direction the mean tumor movement was 5.1 mm , in the ventrodorsal direction 3.1 mm, and in the lateraldirection 2.6 mm
[31]	2017	Tan *et al*	The errors of image-guided registration using 4D-CBCT and 3D-CBCT on the X, Y, Z axes, and 3D space were 0.80 ± 0.21 mm and 1.08 ± 0.25 mm, 2.02 ± 0.46 mm and 3.30 ± 0.53 mm, 0.52 ± 0.16 mm and 0.85 ± 0.24 mm, and 2.25 ± 0.44 mm and 3.59 ± 0.48 mm (all $P < 0.001$), respectively
[32]	2017	Ehrbar *et al*	Compared with the 4D dose calculations, the mid-ventilation and single-phase tracking overestimated the target mean dose (2.3% and 1.3%), respectively
[34]	2016	Garibaldi	The PTV margins used to compensate for residual tumor localization errors were 3.1, 3.5 and 3.3 mm in the LR, SI and AP directions, respectively
[7]	2016	Wang *et al*	Position errors after correction in Left–right, Anterior–posterior and Cranial–caudal were 0.22 cm, 0.16 cm and 0.19 cm, respectively
[36]	2016	Ariyaratne *et al*	Under the use of IGRT, the population mean setup error was 0.01 cm (left–right), 0.05 cm (supero-inferior) and 0.13 cm (antero-posterior)

mDIBH: Moderate deep inspiration breath hold; IGRT: Image-guided radiotherapy; PTV: Planned target volume.

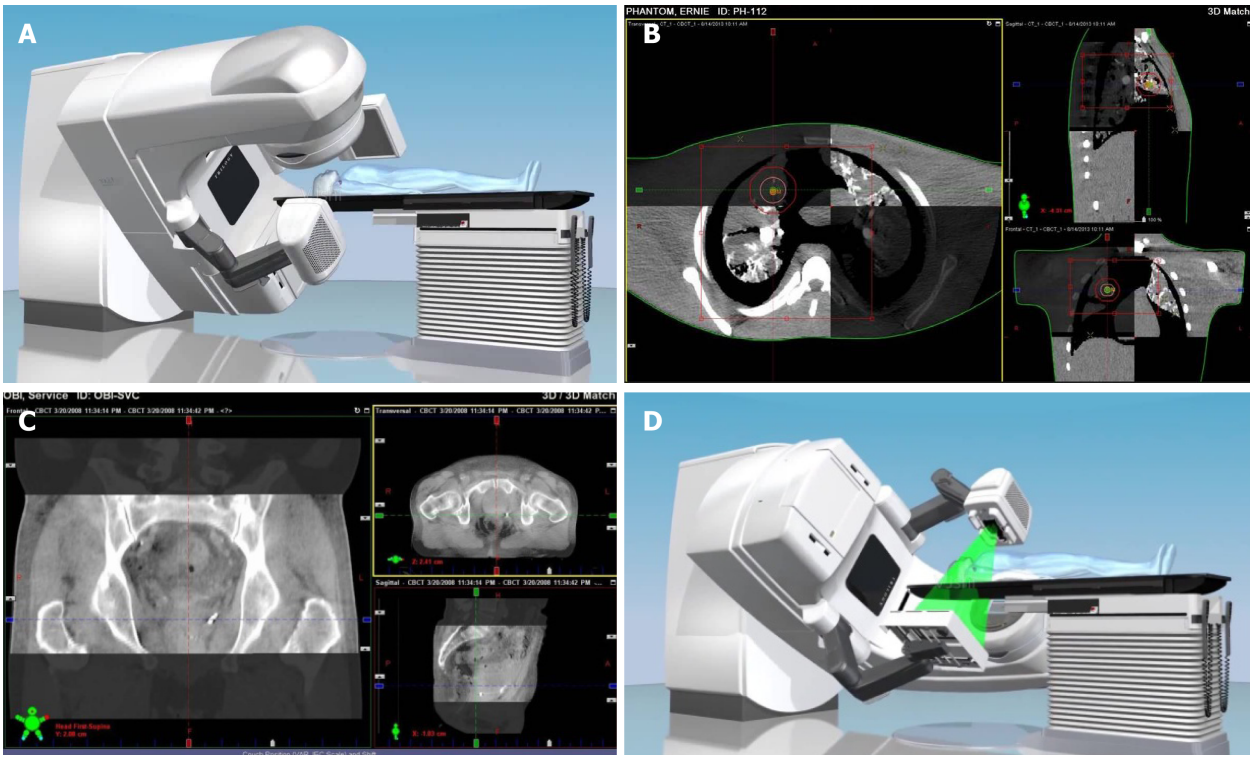

Figure 1 Images of computed tomography. A: The placement of cone beam computed tomography; B: Chest image fusion; C: Pelvic image fusion; D: Radiotherapy after correction with image-guided radiotherapy.

REFERENCES

1 **Glatzer M**, Elicin O, Ramella S, Nestle U, Putora PM. Radio(chemo)therapy in locally advanced nonsmall cell lung cancer. *Eur Respir Rev* 2016; **25**: 65-70 [PMID: 26929423 DOI: 10.1183/16000617.0053-2015]

2 **Holmes T**. *Image-Guided Radiotherapy (IGRT)*. In: Speer TW, Knowlton CA, Mackay MK. Encyclopedia of Radiation Oncology. Springer Berlin Heidelberg 2013; 364-364

3 **Vilotte F**, Antoine M, Bobin M, Latorzeff I, Supiot S, Richaud P, Thomas L, Leduc N, Guérif S, Iriondo-Alberdi J, de Crevoisier R, Sargos P. Post-Prostatectomy Image-Guided Radiotherapy: The Invisible Target Concept. *Front Oncol* 2017; **7**: 34 [PMID: 28337425 DOI: 10.3389/fonc.2017.00034]

4 **Siegel R**, Naishadham D, Jemal A. Cancer statistics, 2012. *CA Cancer J Clin* 2012; **62**: 10-29 [PMID: 22237781 DOI: 10.3322/caac.20138]

5 **Delaney G**, Jacob S, Featherstone C, Barton M. The role of radiotherapy in cancer treatment: estimating optimal utilization from a review of evidence-based clinical guidelines. *Cancer* 2005; **104**: 1129-1137 [PMID: 16080176 DOI: 10.1002/cncr.21324]

6 **Moon SH**, Cho KH, Lee CG, Keum KC, Kim YS, Wu HG, Kim JH, Ahn YC, Oh D, Lee JH. IMRT vs. 2D-radiotherapy or 3D-conformal radiotherapy of nasopharyngeal carcinoma: Survival outcome in a Korean multi-institutional retrospective study (KROG 11-06). *Strahlenther Onkol* 2016; **192**: 377-385 [PMID: 26972085 DOI: 10.1007/s00066-016-0959-y]

7 **Wang SW**, Ren J, Yan YL, Xue CF, Tan L, Ma XW. Effect of image-guided hypofractionated stereotactic radiotherapy on peripheral non-small-cell lung cancer. *Onco Targets Ther* 2016; **9**: 4993-5003 [PMID: 27574441 DOI: 10.2147/OTT.S101125]

8 **De Los Santos J**, Popple R, Agazaryan N, Bayouth JE, Bissonnette JP, Bucci MK, Dieterich S, Dong L, Forster KM, Indelicato D, Langen K, Lehmann J, Mayr N, Parsai I, Salter W, Tomblyn M, Yuh WT, Chetty IJ. Image guided radiation therapy (IGRT) technologies for radiation therapy localization and delivery. *Int J Radiat Oncol Biol Phys* 2013; **87**: 33-45 [PMID: 23664076 DOI: 10.1016/j.ijrobp.2013.02.021]

9 **Arcangeli S**, Falcinelli L, Bracci S, Greco A, Monaco A, Dognini J, Chiostrini C, Bellavita R, Aristei C, Donato V. Treatment outcomes and patterns of radiologic appearance after hypofractionated image-guided radiotherapy delivered with helical tomotherapy (HHT) for lung tumours. *Br J Radiol* 2017; **90**: 20160853 [PMID: 28256158 DOI: 10.1259/bjr.20160853]

10 **Mao W**, Speiser M, Medin P, Papiez L, Solberg T, Xing L. Initial application of a geometric QA tool for integrated MV and kV imaging systems on three image guided radiotherapy systems. *Med Phys* 2011; **38**: 2335-2341 [PMID: 21776767 DOI: 10.1118/1.3570768]

11 **Arns A**, Blessing M, Fleckenstein J, Stsepankou D, Boda-Heggemann J, Simeonova-Chergou A, Hesser J, Lohr F, Wenz F, Wertz H. Towards clinical implementation of ultrafast combined kV-MV CBCT for IGRT of lung cancer : Evaluation of registration accuracy based on phantom study. *Strahlenther Onkol* 2016; **192**: 312-321 [PMID: 26864049 DOI: 10.1007/s00066-016-0947-2]

12 **Wang ZQ**, Li RQ, Zhang Y. Progress in Research of Adaptive Radiation Therapy for Head and Neck Cancer. Zhongguo Aizheng Zazhi. 2016; 131-134 [DOI: 10.3969/j.issn.1007-3969.2014.12.012]

13 **Wang D**, Sha XY, Lin HL. Evaluations of set-up errors and target margins for super and middle part of esophageal carcinoma in image guided radiotherapy. *Zhongguo Fangshe Yixue Yu Fanghu Zazhi* 2014; **34**: 610-612 [DOI: 10.3760/cma.j.issn.0254-5098.2014.08.012]

14 **Li Q**, Kim J, Balagurunathan Y, Liu Y, Latifi K, Stringfield O, Garcia A, Moros EG, Dilling TJ, Schabath MB, Ye Z, Gillies RJ. Imaging features from pretreatment CT scans are associated with clinical outcomes in nonsmall-cell lung cancer patients treated with stereotactic body radiotherapy. *Med Phys* 2017; **44**: 4341-4349 [PMID: 28464316 DOI: 10.1002/mp.12309]

15 **Buckley JG**, Wilkinson D, Malaroda A, Metcalfe P. Investigation of the radiation dose from cone-beam CT for image-guided radiotherapy: A comparison of methodologies. *J Appl Clin Med Phys* 2018; **19**: 174-183 [PMID: 29265684 DOI: 10.1002/acm2.12239]

16 **Rotolo N**, Floridi C, Imperatori A, Fontana F, Ierardi AM, Mangini M, Arlant V, De Marchi G, Novario R, Dominioni L, Fugazzola C, Carrafiello G. Comparison of cone-beam CT-guided and CT fluoroscopy-guided transthoracic needle biopsy of lung nodules. *Eur Radiol* 2016; **26**: 381-389 [PMID: 26045345 DOI: 10.1007/s00330-015-3861-6]

17 **Elsayad K**, Kriz J, Reinartz G, Scobioala S, Ernst I, Haverkamp U, Eich HT. Cone-beam CT-guided radiotherapy in the management of lung cancer: Diagnostic and therapeutic value. *Strahlenther Onkol* 2016; **192**: 83-91 [PMID: 26630946 DOI: 10.1007/s00066-015-0927-y]

18 **Cui QL**, Sun Y, Zhong W, Chen YZ, Zhao YX. Meta-analysis of dosemetriccomparision between helical tomotherapy and intensity-modulated radiotherapy for early-stage postoperative breast cancer. *Cancer Res Clin* 2016; **28**: 828-832 [DOI: 10.3760/cma.j.issn.1006-9801.2016.12.009]

19 **Zhang SX**, Lin SQ. New progress in radiotherapy of NSCLC guided by multimodality medical imaging. *Oncology Progress* 2013; **11**: 520-524

20 **De Bari B**, Jumeau R, Bouchaab H, Vallet V, Matzinger O, Troussier I, Mirimanoff RO, Wagner AD, Hanhloser D, Bourhis J, Ozsahin EM. Efficacy and safety of helical tomotherapy with daily image guidance in anal canal cancer patients. *Acta Oncol* 2016; **55**: 767-773 [PMID: 27034083 DOI: 10.3109/0284186X.2015.1120886]

21 **Remouchamps VM**, Vicini FA, Sharpe MB, Kestin LL, Martinez AA, Wong JW. Significant reductions in heart and lung doses using deep inspiration breath hold with active breathing control and intensity-modulated radiation therapy for patients treated with locoregional breast irradiation. *Int J Radiat Oncol Biol Phys* 2003; **55**: 392-406 [PMID: 12527053 DOI: 10.1016/S0360-3016(02)04143-3]

22 **Muralidhar KR**, Sha RL, Rout BK, Murthy PN. Advantage of using deep inspiration breath hold with active breathing control and image-guided radiation therapy for patients treated with lung cancers. *Int J Cancer Ther Oncol* 2015; **3**: 1-7 [DOI: 10.14319/ijcto.0302.1]

23 **Chang Q**, Lin MZ, Wang XH. Advances in radiotherapy for non-small cell lung cancer guided by image. *Zhongliu Jichu Yu Linchuang* 2014; **27**: 183-184

24 **Jiang SB**, Wolfgang J, Mageras GS. Quality assurance challenges for motion-adaptive radiation therapy: gating, breath holding, and four-dimensional computed tomography. *Int J Radiat Oncol Biol Phys* 2008; **71**: S103-S107 [PMID: 18406905 DOI: 10.1016/j.ijrobp.2007.07.2386]

25 **Bernatowicz K**, Keall P, Mishra P, Knopf A, Lomax A, Kipritidis J. Quantifying the impact of respiratory-gated 4D CT acquisition on thoracic image quality: a digital phantom study. *Med Phys* 2015; **42**: 324-334 [PMID: 25563272 DOI: 10.1118/1.4903936]

26 **Hof H**, Herfarth KK, Münter M, Essig M, Wannenmacher M, Debus J. The use of the multislice CT for the determination of respiratory lung tumor movement in stereotactic single-dose irradiation. *Strahlenther Onkol* 2003; **179**: 542-547 [PMID: 14509953 DOI: 10.1007/s00066-003-1070-8]

27 **Moorees J**, Bezak E. Four dimensional CT imaging: a review of current technologies and modalities. *Australas Phys Eng Sci Med* 2012; **35**: 9-23 [PMID: 22302463 DOI: 10.1007/s13246-012-0124-6]

28 **Liu Q**, Li N, Sun B. Effect of 4D-CT reconstruction technique in accurate radiotherapy for hepatocellular carcinoma. *Weichang Bingxue He Ganbingxue Zazhi* 2016; **25**: 885-888

29 **Zhang SX**, Chen GJ, Zhou LH, Yang KC, Lin SQ. Influences of Motion Artifacts on Three-Dimensional Reconstruction Volume and Conformal Radiotherapy Planning. *Zhongguo Shengwu Yixue Gongcheng Xuebao* 2007; **16**: 123-130

30 **Lu XG**, Ohtani H. The research of respiratory movement induced hepatic tumor motion in radiotherapy by use of a cone-beam CT under the fluoroscopic mode. *Riben Weisheng Kexueyuan Yuanbao* 2017; **16**: 133-139 [DOI: 10.24531/jhsaiih.16.3_133]

31 **Tan Z**, Liu C, Zhou Y, Shen W. Preliminary comparison of the registration effect of 4D-CBCT and 3D-CBCT in image-guided radiotherapy of Stage IA non-small-cell lung cancer. *J Radiat Res* 2017; **58**: 854-861 [PMID: 28992047 DOI: 10.1093/jrr/rrx040]

32 **Ehrbar S**, Jöhl A, Tartas A, Stark LS, Riesterer O, Klöck S, Guckenberger M, Tanadini-Lang S. ITV, mid-ventilation, gating or couch tracking - A comparison of respiratory motion-management techniques based on 4D dose calculations. *Radiother Oncol* 2017; **124**: 80-88 [PMID: 28587761 DOI: 10.1016/j.radonc.2017.05.016]

33 **Jurkovic I**, Stathakis S, Li Y, Patel A, Vincent J, Papanikolaou N, Mavroidis P. SU-E-J-79: Internal Tumor Volume Motion and Volume Size Assessment Using 4D CT Lung Data. *Med Phys* 2014; **41** (6 Part 7): 173-173 [DOI: 10.1118/1.4888131]

34 **Garibaldi C**, Piperno G, Ferrari A, Surgo A, Muto M, Ronchi S, Bazani A, Pansini F, Cremonesi M, Jereczek-Fossa BA, Orecchia R. Translational and rotational localization errors in cone-beam CT based image-guided lung stereotactic radiotherapy. *Phys Med* 2016; **32**: 859-865 [PMID: 27289354 DOI: 10.1016/j.ejmp.2016.05.055]

35 **Nguyen NP**, Kratz S, Chi A, Vock J, Vos P, Shen W, Vincent VH, Ewell L, Jang S, Altdorfer G, Karlsson U, Godinez J, Woods W, Dutta S, Ampil F; International Geriatric Radiotherapy Group. Feasibility of image-guided radiotherapy and concurrent chemotherapy for locally advanced nonsmall cell lung cancer. *Cancer Invest* 2015; **33**: 53-60 [PMID: 25634242 DOI: 10.3109/07357907.2014.1001896]

36 **Ariyaratne H**, Chesham H, Pettingell J, Alonzi R. Image-guided radiotherapy for prostate cancer with cone beam CT: dosimetric effects of imaging frequency and PTV margin. *Radiother Oncol* 2016; **121**: 103-108 [PMID: 27576431 DOI: 10.1016/j.radonc.2016.07.018]

37 **Rudat V**, Nour A, Hammoud M, Alaradi A, Mohammed A. Image-guided intensity-modulated radiotherapy of prostate cancer: Analysis of interfractional errors and acute toxicity. *Strahlenther Onkol* 2016; **192**: 109-117 [PMID: 26545764 DOI: 10.1007/s00066-015-0919-y]

38 **Verma V**, Shostrom VK, Zhen W, Zhang M, Braunstein SE, Holland J, Hallemeier CL, Harkenrider MM, Iskhanian A, Jabbour SK, Attia A, Lee P, Wang K, Decker RH, McGarry RC, Simone CB 2nd. Influence of Fractionation Scheme and Tumor Location on Toxicities After Stereotactic Body Radiation Therapy for Large (≥ 5 cm) Non-Small Cell Lung Cancer: A Multi-institutional Analysis. *Int J Radiat Oncol Biol Phys* 2017; **97**: 778-785 [PMID: 28244414 DOI: 10.1016/j.ijrobp.2016.11.049]

39 **Verma V**, Shostrom VK, Kumar SS, Zhen W, Hallemeier CL, Braunstein SE, Holland J, Harkenrider

MM, S Iskhanian A, Neboori HJ, Jabbour SK, Attia A, Lee P, Alite F, Walker JM, Stahl JM, Wang K, Bingham BS, Hadzitheodorou C, Decker RH, McGarry RC, Simone CB 2nd. Multi-institutional experience of stereotactic body radiotherapy for large (≥5 centimeters) non-small cell lung tumors. *Cancer* 2017; **123**: 688-696 [PMID: 27741355 DOI: 10.1002/cncr.30375]

Published By Baishideng Publishing Group Inc
7041 Koll Center Parkway, Suite 160, Pleasanton, CA 94566, USA
Telephone: +1-925-2238242
Fax: +1-925-2238243
E-mail: bpgoffice@wjgnet.com
Help Desk: https://www.f6publishing.com/helpdesk
https://www.wjgnet.com